A post-transcriptional program of chemoresistance by AU-rich elements/TTP in cancer quiescence

Sooncheol Lee[1,2,3,4], Douglas Micalizzi[1,2], Samuel S Truesdell[1,3,4], Syed IA Bukhari[1,2,3,4], Myriam Boukhali[1,2], Jennifer Lombardi-Story[1,2], Yasutaka Kato[5], Ipsita Dey-Guha[1,2], Benjamin T. Nicholson[1], Min-Kyung Choo[6], David T. Myers[1], Dongjun Lee[7], Maria A Mazzola[8], Radhika Raheja[8], Adam Langenbucher[1,9], Nicholas J. Haradhvala[1,9,10], Michael Lawrence[1,9,10], Roopali Gandhi[8], David A Sweetser[1,11], David Sykes[2,3,4], Wilhelm Haas[1,2], Daniel A. Haber[1,2,12], Shyamala Maheswaran[1,13], and Shobha Vasudevan[1, 2, 3, 4]*

[1]Massachusetts General Hospital Cancer Center, Harvard Medical School, Boston, MA 02114
[2]Department of Medicine, Massachusetts General Hospital and Harvard Medical School, Boston, MA
[3]Center for Regenerative Medicine, Massachusetts General Hospital, Harvard Medical School, Boston, MA 02114
[4]Harvard Stem Cell Institute, Harvard University, Cambridge, MA 02138
[5]Laboratory of Oncology, Hokuto Hospital, Obihiro, Japan
[6]Cutaneous Biology Research Center, Massachusetts General Hospital and Harvard Medical School, Charlestown, MA 02129
[7]Department of Medicine, Pusan National University School of Medicine, South Korea
[8]Center for Neurological Diseases, Brigham & Women's Hospital, Harvard Medical School, Boston, MA 02115
[9]Department of Pathology, Massachusetts General Hospital, Harvard Medical School, Charlestown, MA 02129
[10]Broad Institute of Harvard & MIT, Cambridge, MA 02142
[11]Department of Pediatrics, Divisions of Pediatric Hematology/Oncology and Medical Genetics, Massachusetts General Hospital, Harvard Medical School, Boston, MA 02114
[12]Howard Hughes Medical Institute, Chevy Chase, MD 20815
[13]Department of Surgery, Massachusetts General Hospital and Harvard Medical School, Charlestown, MA 02129

*Correspondence: Shobha Vasudevan 185 Cambridge St, CPZN4202, Boston MA 02114; Ph: 617-643-3143; vasudevan.shobha@mgh.harvard.edu

Running title: Chemoresistance by AU-rich elements & TTP

Key words: quiescence, chemoresistance, post-transcriptional, AU-rich elements, TTP

Financial statement The study is funded by Cancer Research Institute, D. & M-E Ryder, Leukemia & Lymphoma Society, Smith Family Foundation, R01 GM100202 grants to SV & R01 CA185086. SL was funded by Fund for Medical Discovery fellowship & by a postdoctoral fellowship from the Basic Science Research Program through the National Research Foundation of Korea (2015017218). DAS is funded by R01 CA115772. DAH is funded by Howard Hughes Medical Institute and 2R01 CA129933.

Statement on conflict of Interest Authors declare no conflict of interest.

Notes 6633 words; 7 main & 6 supplemental figures

Abstract

Quiescent (G0) cells are transient cell-cycle-arrested subpopulations in cancers that include dormant cancer stem cells. While leukemic stem cells/minimal-residual-disease were studied transcriptionally, their translation profile and post-transcriptional mechanisms that control their proteome—and thereby, survival—are unknown. We find G0 leukemic cells are chemoresistant, with altered canonical translation and similar proteome and translatome—rather than transcriptome—to cells isolated post-chemotherapy, implicating post-transcriptional regulation in chemoresistance. Mechanistically, we find DNA-damage-responsive-ATM and stress-activated-p38-MAPK/MK2 alter post-transcriptional mechanisms, regulating mRNA-decay-factor, TTP, to increase AU-rich-element-bearing mRNAs. This permits translation of AU-rich-element-bearing pro-inflammatory-cytokine TNFα, and immune modulators (CD47) that promote survival. Co-inhibiting p38-MAPK/MK2 and TNFα—prior to/alongwith chemotherapy—decreases chemoresistance in vivo and in patient samples. Disrupting TTP regulation reduces TNFα and chemoresistance, revealing TTP as a regulator of inflammation-mediated chemoresistance. These studies uncover a pro-inflammatory subpopulation in cancer that enables chemoresistance via DNA-damage- and stress-regulated post-transcriptional mechanisms, and develop a new combination therapy against chemo-survival.

Statement of Significance

These studies reveal the significance of post-transcriptional regulation of inflammatory/immune response in chemoresistance, mediated by AU-rich-elements, mRNA-decay-regulator TTP, and non-canonical translation. These results reveal DNA-damage/stress-induced TTP as a key regulator of inflammation-mediated chemoresistance and developed a new combination therapy to reduce resistance in cell lines, patient samples and *in vivo*.

Introduction

Quiescent (G0) cells are an assortment of reversibly arrested cells, including dormant stem cells, which are found as a clinically relevant subpopulation in cancers (1-4). Such cells are anti-proliferative, anti-differentiation, and anti-apoptotic, and show distinct properties including resistance to harsh conditions (1, 2, 5-10). G0 cells show specific gene expression that may underlie their resistance and other properties (1, 2, 8-10). Analyses from multiple groups revealed some genes up-regulated at the transcriptional level (1, 8, 11). Altered polyadenylation site selection on mRNAs produces longer 3′-untranslated regions (3′UTRs) in G0 compared to proliferating cells— which increases 3′UTR elements that can mediate post-transcriptional gene expression regulation (12). Our previous data demonstrated that translation mechanisms are distinct in G0 leukemic cells, with decreased canonical translation mechanisms and increase in mRNA translation by alternative mechanisms that involve non-canonical translation initiation factors (13) and 3′UTR mediated specific mRNA translation (14). These data suggest that alternate post-transcriptional mechanisms in G0 cancer cells may regulate a distinct translatome to mediate their resistance. Translated genes, post-transcriptional mechanisms involved, and outcomes on cancer persistence remain to be investigated.

We analyzed the translatome and proteome of chemotherapy-surviving G0 cancer cells, focusing on acute monocytic leukemia (AML), to provide comprehensive information that complement and expand previous transcriptome analyses (1, 2, 8, 11, 15, 16), (Fig. 1A-B), to reveal critical genes that are post-transcriptionally regulated for chemo-survival. G0 can be induced by growth factor-deprivation or serum-starvation and other conditions that isolate dormant cancer stem cells in distinct cell types (1, 6, 7). Our data demonstrate that serum-starvation induced G0 AML cells are chemoresistant—similar to

surviving AML cells, isolated after chemotherapy. Chemoresistant cells isolated via serum-starvation, or as surviving cells post-chemotherapy, show inhibition of canonical translation mechanisms, indicating that non-canonical mechanisms express specific mRNAs when these cells are chemoresistant. Consistently, the translatomes and proteomes of serum-starved G0 and chemo-surviving cells show greater similarity than the transcriptome alone. These data indicate a specific post-transcriptional program common between serum-starvation induced G0 cells that exhibit resistance, and chemosurviving cells—which may underlie their shared property of chemoresistance.

We find that chemotherapy and serum-starvation induce DNA damage response (DDR) and p38 MAPK stress signaling that lead to up-regulation of specific genes via post-transcriptional mechanisms (17-19) (20-24). Our data reveal AU-rich elements (AREs) enriched in mRNAs that are up-regulated in G0 and in chemo-surviving cells—due to p38 MAPK activation (22, 25, 26) of MAPKAP2 (MK2) kinase (27-29). MK2 regulates ARE binding mRNA decay and translation repression factor, Zinc finger 36 homolog (ZFP36) or Tristetraprolin (TTP) (27-30). We find that p38 MAPK/MK2 mediated regulation of TTP leads to increased ARE bearing mRNA levels and translation in chemoresistant G0 cells. DNA damage-induced ATM kinase and stress signaling—inhibit canonical translation mechanisms in chemoresistant cells, which permits specific gene translation by non-canonical mechanisms that we observed previously (13, 14). The post-transcriptionally regulated genes expressed in G0 resistant cells, include pro-inflammatory genes of the TNFα/NFκB pathway—which we find increase cell survival genes and are required for chemo-survival. Consistently, decreasing expression of TNFα, by expressing a non-regulatable, active mutant TTP (27-29), reduces chemoresistance. Importantly, correlating with their early induction in serum-starved G0 or chemotherapy-treated cells, pharmacological inhibition of

stress signaling and the key translated inflammatory response gene TNFα—prior to or along with chemotherapy—significantly reduces chemoresistance in AML cell lines, patient samples, and *in vivo*. Our data reveal that DNA damage and stress signaling cause post-transcriptional alterations to produce a specialized gene expression program of pro-inflammatory, immune effectors that elicit chemo-survival.

Results

Serum-starvation or AraC treatment induces a quiescent and chemoresistant state of leukemic cells

To study clinical resistance in cancer, THP1 human AML cells were used as they show significant resistance to cytarabine (31) (cytosine arabinoside, AraC, Fig. S1A), a standard anti-leukemic chemotherapeutic that targets DNA replication and thus proliferating cells (referred to as S+). Our data and others find that serum-starvation of THP1 (13) and other cell lines (1, 8, 11, 32) induces a transient G0 state with known G0 and cell cycle arrest markers expressed (Fig. 1C-D, S1B-C). Such serum-starvation induced G0 cells (referred to as SS) can be returned to the cell cycle upon serum addition (Fig. 1D), verifying that they are quiescent and transiently arrested, unlike senescence or differentiation that are not easily reversed. We find that serum-starvation induced G0 SS cells show resistance to AraC chemotherapy. Serum-grown S+ cells show a dose-dependent decrease in cell viability with AraC as expected, while SS cells persist, indicating their chemoresistance (Fig. 1E).

Chemoresistant cancer cells include cancer stem cells, and are a subpopulation that can be isolated from cancers after treatment with chemotherapy (2, 6-10) that targets and eliminates S+ cells. We find that AraC-surviving THP1 (referred to as AraCS) cells are transiently arrested, like serum-starved SS cells

(Fig. 1C-D, S1B); both AraCS and SS cells survive chemotherapy. AraCS cells recover from their transient arrest upon AraC removal, proliferate (Fig. 1D) and give rise to resistance upon subsequent AraC treatment (Fig. 1E), affirming the reversible G0 arrest state of chemoresistant cells, similar to SS cells (1, 2, 6-10).

Chemoresistant G0 cells induced by SS or AraC have similar translatomes and proteomes that recapitulate gene expression profiles of *in vivo* chemoresistant leukemic and G0 models

We asked whether the underlying gene expression is similarly regulated in both SS and AraC cells, leading to their common property of chemoresistance. We previously observed canonical translation shutdown that allowed non-canonical translation of specific genes in SS cells (13, 14), indicating post-transcriptional changes in such cells. Therefore, to differentiate translationally-regulated from transcriptionally-regulated genes associated with chemoresistance, we profiled AraCS cells and SS cells—and compared them with S+ cells at the proteome, translatome and transcriptome levels using: multiplexed quantitative proteomics (14), microarray analysis of heavy polysome-associated mRNAs (13, 14, 33) for the translatome, and total RNA microarray for the transcriptome (Fig. 1A-B, S1D-F). Consistently, we find that AraCS and SS cells show significantly similar gene expression profiles in their proteomes and translatomes rather than transcriptomes (Fig. 1F). These data suggest that although these chemoresistant G0 cells are isolated via two different methods: therapy survival or serum-starvation, they exhibit a common set of specific genes expressed at the protein level, which could underlie their common characteristic of chemoresistance. These data indicate the relevance of examining the translatome and post-transcriptional regulation of gene expression, in addition to the transcriptome. Time-course translatome analysis revealed that early serum-starved G0 (4 h and 1 day SS) cells are

distinct from late, 2-4 days G0 cells (2-4 days SS are more similar in their translatomes, R^2=0.81, Fig. S1E-F). This is consistent with G0 as a continuum of assorted, arrested states (1), with temporal differences in underlying gene expression in early G0 compared to more homogeneity at late G0.

SS and AraCS cells provide sufficient material to perform concurrent translatome, proteome and transcriptome profiling for post-transcriptional regulation analyses, compared to limited cells from in *vivo* resistance models. To test whether our G0 leukemic cells are relevant models to study chemoresistance and G0, gene expression profiles of AraCS and SS cells were compared to published transcriptome profiles of *in vivo* chemoresistance models, including leukemic stem cells, dormant leukemic cells and chemosurviving cells, as well as to a published G0 model that were isolated by different methods: leukemia stem cells (LSC) from AML (16), dormant leukemic cells (LRC), and minimal residual disease (MRD) from chemotherapy surviving patient samples with acute lymphocytic leukemia (ALL) (15), as well as SS G0 fibroblasts (G0 HFF) (1). Importantly, we find that these published transcriptome signatures for *in vivo* chemoresistance and G0 models were significantly up-regulated in our SS and AraCS cells (referred to as resistant G0 leukemic cells), compared to S+ cells (Fig. 1G, S1G). These data indicate that our resistant G0 leukemic cells are relevant models to study post-transcriptional regulation in chemoresistance as they have similar gene expression profiles to known transcriptional profiles from *in vivo* chemoresistance models.

Altered translation with inhibition of canonical translation mechanisms in resistant G0 leukemic cells

As previously observed in SS cells (13, 34-39), we find overall protein synthesis is reduced at least 2-fold in AraCS, compared to S+ cells (Fig. 2B, S1D). Mechanistically, both rate-limiting steps in canonical translation initiation: recruitment of initiator tRNA, and mRNA cap recognition to recruit mRNAs to ribosomes are inhibited in G0 leukemic cells (Fig. 2A-C). Recruitment of initiator tRNA by eIF2 can be blocked by eIF2α phosphorylation as a stress response (13, 34-39). We find that two eIF2 kinases, PKR and PERK, are activated and increase eIF2α phosphorylation (Fig. 2A, 2C) to inhibit canonical translation initiation in G0 leukemic cells. Our previous data revealed low mTOR activity (14), leading to dephosphorylated and active eIF4EBP (4EBP) (Fig. 2A, 2C) that inhibits cap-dependent translation initiation (40, 41). Low mTOR activity reduces translation of terminal oligopyrimidine tract (TOP) mRNAs such as ribosomal protein mRNAs (40, 42, 43), which we find decreased in SS and AraCS cells (Fig. 2A, 2D). Decreased canonical translation can enable post-transcriptional regulation of specific genes, as observed previously (13, 14) and lead to survival of G0 leukemic cells.

Global translatome analysis shows that inflammatory response genes are selectively translated in resistant G0 cancer cells

We measured the number of genes upregulated at the transcriptome, translatome and proteome levels in resistant G0 leukemic cells, compared to S+ cells. A significantly greater number of genes were upregulated in the translatome (580 genes, Table S1) and proteome (716 genes), compared to the transcriptome (318 genes) as shown in Fig. 2E. Importantly, 70% of upregulated genes (418 out of 580) were increased in the translatome (Fig. 2F) but not in the transcriptome, indicating a common set of specific genes that are post-transcriptionally/translationally expressed. To investigate the biological function of these differentially expressed genes, gene ontology (GO) analysis was performed with each

gene set. Gene categories up-regulated in G0 translatomes include inflammatory response, immune modulators (receptors, antigen presentation and processing genes), cell adhesion, cell migration, lipid biosynthesis and cholesterol pathway genes (Fig. 2G, S2E). Down-regulated genes include RNA processing and ribosome genes, consistent with the limited, specialized gene expression here, as well as decreased DNA repair genes that would permit DNA damage and stress signaling (Fig. 2G). To identify translationally up-regulated genes, we measured the change in ribosome occupancy, RO, which is the ratio of polysome-associated mRNA levels to total mRNA levels of each gene (Fig. 2F, Venn diagram, heat map). We find 180 genes are translationally up-regulated above RNA level changes in G0 ($\Delta RO = RO_{G0} - RO_{proliferating} > 1.5$-fold). These genes include antigen processing and presentation genes (44) (HLA-G, HLA-E) and immune receptors (CD47, Fig. 2F-G, S2I) (45-47) that regulate anti-tumor immune response and are associated with leukemic stem cells and resistance (48, 49).

We asked if this specific gene expression profile in resistant G0 leukemic cells is conserved in G0 cells of other tumors and in normal cells. Therefore, global translatome profiling was conducted in G0 cells from four different cells lines: breast cancer (MCF7, Fig. S2B-D), liver cancer (HEP-G2), and osteosarcoma (U2OS) as well as non-cancerous fibroblasts (HFF) (Fig. S2A, D). Their translatomes were compared with resistant G0 leukemic cells, using GSEA and DAVID tools (Fig. 2H-I, S2E-F). We find that 580 signature genes of resistant G0 leukemic cells (Table S1) were highly conserved at the translatome level in G0 cells of these other cell types (Fig. 2H). As expected for these arrested cells, genes related to cell cycle, ribosome biogenesis, and DNA replication were commonly down-regulated (Fig. 2I, S2E). Importantly, inflammatory response genes were commonly up-regulated in cancer G0 cells but not normal G0 fibroblasts and do not significantly overlap with senescence-associated secretory pathway (SASP) (Fig. 2I, S2G) (50, 51), indicating a specific role in chemoresistant cancer cells. These

results indicate that specialized post-transcriptional mechanisms are enabled in these conditions of decreased canonical translation and lead to common expression of specific genes; in particular, of inflammatory response genes in chemoresistant G0 cancer cells.

Post-transcriptional up-regulation of ARE-bearing mRNAs is mediated by phosphorylation of TTP in resistant G0 leukemic cells

To identify RNA motifs that mediate post-transcriptional regulation, the untranslated regions (UTRs) of differentially expressed genes in G0 leukemic cells were examined. Three UTR elements were found: two 5′UTR elements and a key post-transcriptional regulatory 3′UTR AU-rich element. A GC-rich motif was enriched on 5′UTRs of translationally up-regulated genes ($\Delta RO > 1.5$) and an AU rich motif, on 5′ UTRs of translationally suppressed genes ($\Delta RO < 1.5$), indicating that mRNAs with structured 5′UTRs are highly translated in G0 cells (Fig. S3A-B). Importantly, 3′UTRs of genes in the up-regulated translatome have higher AU-rich elements (AREs) scores, compared to down-regulated translatome (Fig 3A). Over 30% of the translatome signature of G0 leukemic cells bear AREs, including key proinflammatory cytokines/chemokines, such as TNFα (Figs. 3B-D, Table S2) (25). AREs regulate mRNA stability and translation to control expression of critical growth factors and immune genes (52, 53). AREs are involved in mediating specific mRNA decay; however, depending on their associated RNA binding proteins and cellular conditions that signal and modify these interactions, AREs can promote mRNA stability and translation, as in the case of TNFα and other mRNAs in G0 and other conditions (14, 28, 52, 54-56). Consistently, we find that most ARE binding proteins that are RNA decay or translation repression factors (Fig. S3C, S3F) (57, 58), are decreased in SS and AraCS cells. Additionally, we find decrease of the exosome RNA decay complex (Fig. S3D) that is involved in

ribosome processing (59) and ARE mRNA decay (28, 29, 60), and of proteasome factors (61) (Fig. S3E) that are implicated in ARE mRNA decay. A key ARE mRNA decay factor, TTP, was surprisingly increased in G0 leukemic cells (Fig. S3F, 3B-C, 3E-F). TTP phosphorylation is established to increase its levels (28), and results in inability of phospho-TTP to down-regulate ARE mRNA expression; such ARE mRNAs are stabilized and translated (29, 30). Accordingly, we find that TTP is phosphorylated in SS and AraCS cells (Fig. 3F), accounting for its increased levels (Fig. S3F, 3B-C, 3E-F). To test whether phosphorylation of TTP was required for expressed ARE mRNAs in SS and AraCS cells, we over-expressed non-regulatable active mutant TTP that has its key phosphorylation sites (Ser 52, 178) mutated to alanine (TTP-AA). TTP-AA has been shown to dominantly maintain ARE mRNA decay activity and reduce pro-inflammatory cytokines like TNFα in immune cells (28-30). Over-expression of myc-tagged TTP-AA compared to control vector significantly reduced TNFα mRNA in both THP1 and K562 AraCS cells (Fig. 3G), overturning the decay inactivity of endogenous phospho-TTP. These data indicate that inactivation of ARE mRNA decay by TTP phosphorylation (27-29) is a key regulator of pro-inflammatory gene/TNFα expression in chemoresistant G0 cells. These results are consistent with our findings of increased levels and translation of ARE bearing mRNAs—including many pro-inflammatory cytokines (Fig. 2G, 3A-C)—due to decreased ARE decay activity in SS and AraCS cells (Fig. 3F-G, S3C-F).

Activation of p38 MAPK/MK2 phosphorylates TTP to promote expression of ARE-bearing mRNAs in resistant G0 leukemic cells

To investigate how TTP is phosphorylated in resistant G0 leukemic cells, we examined key signaling molecules involved in DNA-damage response (DDR) or stress (20) since chemotherapies like AraC

trigger DNA damage-mediated induction of ATM kinase and stress, which activate p38 MAPK (17-20). P38 MAPK signaling is also activated by G0 and serum-starvation (62). As expected, AraC treatment induced rapid phosphorylation and activation of ATM (Fig. 3H-I) (17-20). Importantly, we find that ATM-mediated DDR leads to phosphorylation and activation of p38 MAPK and its downstream effector, MAPKAPK2 (MK2) (22, 26) on AraC treatment (Fig. 3H-I). MK2 phosphorylates TTP to up-regulate inflammatory gene expression in immune cells (27-29). To examine if MK2 kinase could phosphorylate TTP in resistant G0 leukemic cells, two different inhibitors of p38 MAPK/MK2 were tested. Inhibition of p38 MAPK, using the clinically tested p38 MAPKα/β inhibitor, LY2228820 (LY) (22, 63), or a pan p38 MAPK inhibitor that targets all isoforms, BIRB796 (BIRB) (64), blocks phosphorylation of MK2, which prevents MK2-mediated TTP phosphorylation and reduces TNFα in AraCS cells (Fig. 3J). These results suggest that p38 MAPK/MK2 phosphorylates TTP, resulting in expression of ARE mRNAs such as TNFα in G0 leukemic cells (Fig. 3H). To test if p38 MAPK/MK/TTP regulates TNFα expression via its ARE, a Firefly luciferase reporter bearing the 3′ UTR ARE of TNFα was tested, with Renilla luciferase as co-transfected control. Luciferase activity increased by 2-fold in AraCS cells compared to S+ cells but not when p38 MAPK was inhibited with LY (Fig. 3K). These data suggest that p38 MAPK/MK2/TTP axis up-regulates specific gene expression via AREs in G0 leukemic cells. These results are consistent with our findings of increased ARE bearing, pro-inflammatory factor mRNA levels and translation—due to decreased ARE mRNA decay by the ATM-p38 MAPK-MK2-TTP axis (Fig. 3H) that is induced by stress and DNA damage signaling due to serum-starvation and chemotherapy (26).

Transiently activated p38 MAPK/MK2 in early G0—at early times of serum-starvation and chemotherapy treatment—promotes chemoresistance

We noted that p38 MAPK and MK2 were transiently phosphorylated, at early times upon induction of G0 cells with SS or AraC treatment (Fig. 3I and 4A-B). To investigate whether early activation of p38 MAPK/MK2 impacted AraC resistance, p38 MAPK was pharmacologically inhibited *before* (or along with) as well as *after* treatment with AraC—and then chemo-survival was measured using multiple assays, including cell death and two cell viability assays (Fig. 4C-E). Inhibition of p38 MAPK/MK2 with BIRB (Fig. 4D) or LY (Fig. 4E), one day *after* treatment with AraC, does not show any significant reduction in survival of AraC-resistant cells. Critically, inhibition of p38 MAPK/MK2 at early time points—4h-1 day *prior to* AraC treatment or *along with* AraC treatment—increased apoptosis and reduced survival of 70% of AraC-resistant cells (Fig. 4D-E). As a control, p38 MAPK inhibition alone does not affect viability of S+ cells that are not treated with AraC (Fig. 4D-E). These results suggest that p38 MAPK/MK2 is rapidly activated upon AraC treatment to turn on downstream survival genes at early times. Therefore, to overcome AraC resistance effectively, p38 MAPK/MK2 should be targeted at early time points before it induces downstream survival pathways that would dampen the effect of anti-inflammatory therapeutics. Consistently, sequential treatment with p38 MAPK inhibitor, LY, followed by AraC showed a dramatic reduction (50-70%) in chemo-survival in multiple AML cell lines but not in non-cancerous cells (Fig. 4F, CD34+), as these pathways (MAPK, inflammatory genes) are not up-regulated in non-cancerous G0 (Fig. 2I). When treated with p38 MAPK inhibitor alone, viability of S+ cells in multiple AML cell lines remained unchanged, indicating the synergism of AraC and p38 MAPK inhibitors on resistant leukemic cells (Fig. 4F). Interestingly, p38 MAPK inhibition eliminated resistant cells more significantly at increasing concentrations of AraC (Fig. 4G). Treatment with high concentrations of AraC would increase the number of cells induced into the resistant G0 state with

induction of p38 MAPK; therefore, inhibition of this pathway is more effective at high concentrations of AraC. Conversely, even low concentration of p38 MAPK inhibitor, BIRB, was sufficient to reduce chemoresistance (Fig. S4B). Activation of p38 MAPK/MK2 can induce resistance by arresting the cell cycle (22, 25, 26); however, p38 MAPK/MK2 inhibition did not affect the cell cycle in resistant G0 leukemic cells (Fig. S4A), indicating a distinct mechanism of resistance by p38 MAPK/MK2 in G0. These data uncover early and rapid activation of a p38 MAPK/MK2 pathway that enables chemo-survival of G0 leukemic cells—in part, through inhibition of TTP activity that enables expression of pro-survival, pro-inflammatory genes like TNFα (Fig. 5A). Pharmacological inhibition of this early-activated p38 MAPK/MK2 pathway *prior to* and along with chemotherapy reduces resistance; in contrast, post-chemotherapy inhibition of p38 MAPK/MK2 is not effective, as at later time points their downstream effectors of cell survival genes are already on.

Activation of p38 MAPK/MK2 promotes chemoresistance *via* inactivation of TTP and subsequent up-regulation of TNFα

We investigated the mechanism by which p38 MAPK/MK2 promotes chemo-survival in G0 leukemic cells. As shown in Fig. 3G-K, p38 MAPK/MK2 phosphorylates and inactivates TTP, leading to increased production of TNFα. TNFα activates the NFκB pathway that increases anti-apoptotic gene expression as a stress response to promote cell survival (65-67). Importantly, our translatome analysis shows a significant increase in TNFα, TNFα receptors (Fig. S5A) and NFκB signaling (Fig. 5B), including anti-apoptotic BCL family members (Fig. S5B) (67-69), indicating that TNFα-mediated inflammatory response may cause chemoresistance. To examine the role of the TTP-TNFα axis in AraC resistance, we expressed non-phosphorylatable TTP mutant (TTP-AA) that is active in ARE mRNA

decay and inhibits TNFα (Fig. 3G). Importantly, we find that TTP-AA expression reduces survival of AraC-resistant cells (Fig. 5C). These data suggest that TTP phosphorylation and inactivation—by p38 MAPK/MK2—enables chemo-survival through expression of ARE-bearing pro-inflammatory genes like TNFα.

Inhibition of TNFα/NFκB—prior to or at the same time as chemotherapy—decreases resistance, correlating with transient, early increase in expression of TNFα/NFκB in early G0

TTP may have other targets apart from TNFα. To verify that TTP regulates chemoresistance via targeting TNFα, we created a stable cell line expressing an inducible shRNA against TNFα. As shown in Fig. 5D, induction of TNFα depletion prior to AraC treatment effectively reduced AraC resistance, compared to after AraC treatment, while no effect was observed with TNFα depletion alone without AraC. In contrast, addition of recombinant TNFα enhanced survival of AraC-treated cells (Fig. 5D). TNFα-mediated chemoresistance is not due to arrested cell cycle as TNFα treatment without subsequent AraC does not alter the cell cycle (Fig. S5C). These data suggest that phosphorylation of TTP and subsequent expression of TNFα, which are induced by p38 MAPK/MK2, are responsible for survival of G0 leukemic cells.

TNFα can also be inhibited pharmacologically with the inhibitor Pirfenidone (PFD, Fig. 5A) that can block TNFα translation, reduce inflammatory factors, and is clinically used for inflammatory disease like fibrosis (22, 70, 71). PFD decreases TNFα at the translatome and proteome levels in G0 leukemic cells (Fig. 5E). Our observation of early activation of p38 MAPK/MK2 (Fig. 4A-B) suggested that TNFα could be rapidly up-regulated upon G0 induction. Time-course translatome analysis affirmed that

TNFα is most significantly increased (16-fold) at the earliest time point of 4 h after serum-starvation or AraC treatment (Fig. 5B), causing early expression of NFκB target genes including cell survival genes (Fig. 5B and S5B). Consistently, PFD treatment at least 18 hours *prior to* or along with AraC or serum-starvation significantly reduced viability of G0 leukemic cells but failed to reduce resistance when added *after* AraC treatment (Fig. 5F, S5D). PFD treatment alone does not affect the viability of untreated S+ cells, indicating that the cytotoxic effect of PFD is specific to G0 leukemic cells (Fig. 5F). Similar results were observed in MCF7 cells, where PFD reduced doxorubicin resistance (Fig. S5H). These data indicate that activation of the inflammatory pathway is an early event in G0 cells, which leads to resistance, and needs to be inhibited early to preclude downstream survival regulators.

PFD treatment reduced chemotherapy survival in multiple AML cell lines but not all leukemia types (Fig. 5G, AML cell lines versus chronic myelogenous leukemia K562). Since PFD could affect targets other than TNFα to reduce resistance (22, 70, 71), we tested the effect of PFD along with shTNFα depletion together, prior to AraC chemotherapy, in comparison to individual treatments: an additive effect would not be observed if PFD affects chemosurvival through TNFα and not via other targets. Co-treatment with PFD and TNFα shRNA prior to AraC did not show an additive effect of reducing survival compared to PFD treatment alone, indicating that the effect of PFD was mediated through TNFα inhibition (Fig. S5E). Similarly, we find that inhibition of TNFα-induced NFκB, with NFκB inhibitor, BAY11-7082 (72) to block downstream anti-apoptotic response, prior to or along with AraC or serum-starvation, decreases survival; treatment after chemotherapy or serum-starvation had no effect as observed with upstream TNFα inhibitor PFD (Fig. 5H). These data suggest that the TNFα/NFκB inflammatory pathway is upregulated as an early survival pathway in G0 cells, which increases chemo-survival. In accord with the transient increase of inflammatory genes at early times in these G0 cells

after chemotherapy or serum-starvation, we find that treatment with inflammation inhibitors (PFD or BAY11-7082) or TNFα shRNA *prior to* and continued with chemotherapy significantly reduces chemoresistance—while treatment post-chemotherapy, fails to reduce resistance.

Co-inhibition of p38 MAPK and TNFα sensitizes resistant leukemic cells to AraC treatment by reducing TNFα and activating a pro-apoptotic JNK pathway

Although chemoresistant cells are sensitive to individual inhibition of either TNFα or p38 MAPK by PFD or LY respectively, a substantial proportion of cells still survived (Fig. 4F, 5G). Therefore, we asked if co-inhibition of p38 MAPK and TNFα with LY *and* PFD respectively, could eliminate the remaining resistant cells. We find that individual treatment, with low concentrations of LY or PFD (half of the concentrations used in Fig. 4-5), prior to or along with AraC, reduces approximately 50% of surviving leukemic cells (Fig. 6A-B). Importantly, the combination of PFD *and* LY2228820 prior to AraC treatment–called PLA therapy–eliminates about 90% of chemoresistant cells in multiple AML cell lines (Fig. 6A-C). Furthermore, PLA therapy decreased colony formation capacity of leukemic cells on methylcellulose by 10-fold, compared to AraC-treatment alone (Fig. 6D). These data indicate a severe loss of stem cell capacity of leukemic cells treated with PLA therapy. In contrast, in the absence of AraC treatment, the combination of PFD and LY2228820 did not affect cell viability, apoptosis and colony formation capacity, indicating the synergistic effect between AraC and anti-inflammatory drugs (Fig. 6A-D). Despite the fact that stromal niche cells have been shown to protect leukemic cells from chemotherapy (73), we find that AML cells co-cultured with stromal cells remained sensitive to PLA therapy (Fig S5F).

We investigated the molecular mechanism by which PLA therapy enhanced chemosensitivity. First, TNFα depletion reduces chemoresistance (Fig. 5D). LY destabilizes TNFα mRNAs by TTP dephosphorylation (28) (Fig. 3J), while PFD was shown to suppress TNFα selectively at the translation level (71); consistently, PFD treatment in chemoresistant G0 leukemic cells reduced TNFα at the translatome level but not at the RNA level (Fig. S5G). Therefore, in PLA therapy, phosphorylation of p38 MAPK target MK2 is decreased by LY, diminishing TTP phosphorylation and reducing TNFα mRNA levels (Fig. 3G-J) (28)—and additionally, due to inhibition of TNFα translation by PFD, TNFα remains more effectively blocked, compared to individual drug treatments (Fig. 6E). Second, we investigated c-Jun N terminal kinase (JNK) that can promote apoptosis depending on stimulus and cell type (74). Phosphorylation of JNK was enhanced in cells treated with PLA therapy, compared to single-drug treatments (Fig. 6E). JNK inhibitor, JNK-IN-8 partially reversed apoptosis of PLA therapy-treated cells, but did not affect the viability of cells not treated with PLA (Fig. 6F). Together, these results suggest that PLA therapy reduces TNFα and promotes a pro-apoptotic JNK pathway, leading to apoptosis of chemoresistant cells.

PLA therapy reduces chemoresistance in primary AML cells *ex vivo* and *in vivo*

To test the anti-leukemic activity of PLA therapy in primary AML (75), primary cells from AML patients as well as two murine AML models driven by Hoxa9/Meis1 or MLL/AF9 (SI Methods), were used. When either p38 MAPK or TNFα was inhibited prior to AraC treatment, moderate apoptosis of chemoresistant cells was observed in primary AML cells (Fig. 7A-B). Importantly, co-inhibition of p38 MAPK and TNFα by PLA therapy (pre-treatment before AraC) significantly reduced AraC resistance in fourteen out of fifteen AML patient samples as well as in primary cells from two AML mouse models *ex vivo* (Fig. 7A-B). In contrast, the viability of normal CD34+ cells from healthy donors was not affected

by treatment with LY or PFD (Fig. 4F, 7A-B), consistent with clinical studies that have shown that PFD and LY have acceptable safety and tolerance (63, 70). To further investigate the therapeutic potential of PLA therapy *in vivo*, human AML cells expressing luciferase (MOLM13-Luc, SI Methods) were intravenously or subcutaneously injected into NSG mice. After confirmation of engraftment by measuring tumor volume or bioluminescent imaging (BLI), the mice were treated with PLA therapy or AraC for two weeks. Consistent with *ex vivo* results (Fig. 6B), PLA therapy significantly decreased the leukemic burden and tumor volume by 6-fold, compared to AraC treatment alone (Fig. 7C-D). Next, we tested PLA therapy in C57BL/6 mice engrafted with primary Hoxa9/Meis1 leukemia cells expressing luciferase. These mice were treated with PLA therapy or AraC. Consistently, BLI shows that PLA therapy eliminated 78% or 96% of chemoresistant cells in a dosage-dependent manner (Fig. 7E-F) and extended mice survival by 7 days (Fig. 7F). In the absence of AraC treatment, the combination of PFD and LY2228820 did not affect leukemic burden, suggesting that cytotoxic effects of this combination are limited to AraC-resistant cells, rather than proliferating cells (Fig. 7G). Together, these results suggest PLA therapy has potential for improving AraC-mediated apoptosis in AML.

Discussion

G0 cells are a transiently arrested, clinically relevant subpopulation in cancers (1, 2, 5-10). Our previous data and others, revealed altered gene expression mechanisms in G0 leukemic cells, at the post-transcriptional (8, 12) and translational levels (13, 14, 32). This would lead to a distinct gene expression profile to enable G0 cell survival in harsh conditions. G0 cells are resistant to stress conditions like serum-starvation, with transient inhibition of apoptosis, and proliferation (1, 11, 32), which are features required for cells to survive chemotherapy. Importantly, we find that serum-starved leukemic SS cells

exhibit chemoresistance (Fig. 1E); consistently, true chemo-surviving AraCS cells are transiently arrested and chemoresistant (Fig. 1D-E, S1B-C). In accord, we find that SS cells are similar in translatome and proteome to AraCS cells (Fig. 1F), indicating that consistent with their common features of G0 arrest and chemosurvival, they show similar post-transcription gene expression. Published transcriptional signatures of G0 fibroblasts, and of leukemic stem cells and other in vivo chemoresistance leukemic models (1, 2, 8, 11, 15, 16), are also highly expressed in SS and AraCS cells (Fig. 1G, S1G). Thus, the common G0 resistance gene expression profile observed in AraCS and SS G0 cells—distinct from neighboring proliferating tumor cells—likely comprises genes that control survival and resistance. These data revealed that in addition to known transcriptional profiles, altered post-transcriptional and translation mechanisms in G0 resistant cells contribute to their unique gene expression profile that underlies their chemoresistance.

Our findings reveal the importance of DNA damage and stress signaling that can initiate a pro-inflammatory response that causes survival instead of cytotoxicity (Fig. 4-6, S4-S6). Differential genomic instability in cancers would lead to distinct subpopulations within a tumor with disparate DDR and stress signaling (17-19) that we find, enables their chemotherapy survival via pro-inflammatory cytokines. Cytokines upregulated in SS and AraCS cells do not significantly match SASP (50, 51) (Fig. S2G). This is consistent with differences between G0 and senescence (1)—with low mTOR activity (Fig. 2A-C, I, S2E) (14) and mutated p53 in these G0 cells—unlike high mTOR activity and p53 in senescence (32). These data indicate that a quiescence- and resistance-specific set of pro-inflammatory genes are expressed in these resistant cells. These include inflammatory cytokines (Fig. 2F-G) that promote downstream NFκB activated pro-survival target genes (65-67) including BCL family members

of anti-apoptotic genes (67-69) (Fig. 5A-B, S5A-B). Treatment with reagents against these resistance-enabling immune regulators *after* chemotherapy is not very effective as the downstream survival effectors have already been induced; thus, targeting their upstream cytokine regulators would not be effective at this later time (Fig. 4A-B, 4D-E, 5F-H, S5D, 6B). Thus, treatment with reagents that block these resistance pathways *prior to* (and continued with) or along with chemotherapy, enables the most effective reduction of resistance, as they prevent further enrichment of such resistant cells by blocking induction of pro-survival signaling.

AraC is a nucleotide analog and inhibits replication, which triggers DDR (31). Increasing the concentration of AraC would cause increased DDR and downstream p38 MAPK signaling (17-19) and should lead to more cells expressing this inflammatory pathway that enables resistance—and thus pushes more cells into the inflammatory phase that can be targeted by inhibitors. Consistently, increased AraC treatment leads to more cells in the inflammatory phase that can be targeted by LY, leading to more significant loss of resistance (Fig. 4G). Non-cancerous cells do not show this pathway (Fig. 2I) and are not affected by inhibitors (Fig. 4F, 7A). These data suggest that certain chemotherapies and stresses like serum-starvation induce stress signaling (Fig. 4A-C) and enrich for resistant G0 cells—in addition to pre-existing subpopulations with genomic instability that trigger DDR and stress (17-19). Importantly, this resistance mechanism can be blocked to significantly decrease resistance to AraC, not only in different AML cell lines (Fig. 4C-G, 6B) but also in vivo in AML xenograft and mouse models (Fig. 7C-G) as well as in multiple patient-derived AML samples—without affecting normal cells (Fig. 7A)—supporting their potential applicability as a therapeutic target against chemoresistance in AML.

We find key signaling pathways (Fig. S6), mediated by AraCS and SS treatments (Fig. 4A-B, 5A-B), which alter post-transcriptional and translational gene expression to enable resistance. These include: 1. DNA damage ATM (17-19) and stress activated p38 MAPK signaling that in turn promotes (Fig. 4A-B) MK2 (22, 26); MK2 post-transcriptionally upregulates ARE bearing mRNAs (27-29) (Fig. 3G-K, 4A-B), including proinflammatory cytokines like TNFα (65, 66) that activate downstream anti-apoptosis signals (Fig. 5A-B, S5A-B) (67-69) to promote resistance (Fig. 5-7). 2. ATM mediated suppression of mTOR activity (17, 18) to inhibit canonical translation via 4EBP dephosphorylation that enables non-canonical translation (14) (Fig. 2A-C); this results in specific translation of pro-inflammatory cytokines (Fig. 3A-D) and immune modulators (44) (HLA-G, CD47, Fig. 2F-G, S2I) (45-47) that regulate anti-tumor immune response and are associated with resistance (48, 49). 3. UPR stress signaling that can be induced by p38 MAPK (62) and DNA damage (23, 24); this inhibits canonical translation via PERK phosphorylation of eIF2α and enables non-canonical specific mRNA translation (Fig. 2A-D, S2H)—which also increases inflammation and blocks apoptosis to enable chemoresistance (23, 24). Blocking the p38 MAPKα/β pathway with LY (22, 63), in combination with the anti-inflammatory PFD (22, 70, 71) that blocks downstream TNFα expression (70, 71) (Fig. 5A, E, S5G)—prior to (and continued with) AraC chemotherapy—lead to effective loss of chemoresistance in multiple AML cell lines (Fig. 6B), in tumors *in vivo* in AML mouse models (Fig. 7C-G), and in patient samples (Fig. 7A), validating their ability to reduce resistance and tumors *in vitro* and *in vivo*. LY destabilizes TNFα mRNA by TTP dephosphorylation (Fig. 3J) (28), while PFD suppresses TNFα selectively at the translation level (71) (Fig. S5G) and thus enables PLA combination therapy to more effectively sustain reduction in resistance than the individual drugs. Apart from its effect on TNFα translation, PFD blocks inflammation regulator (21, 76) p38 MAPKγ that can be increased upon p38MAPKα/β inhibition, preventing feedback reactivation of inflammation, and enabling PLA combination therapy to remain more efficacious than

the individual drugs. Consistently, in the combination treatment with LY and PFD, LY decreases phosphorylation of MK2 by p38 MAPK, reducing TTP phosphorylation and TNFα RNA levels (Fig. 3G-J) (28); additionally, TNFα translation is inhibited by PFD, resulting in chemo-survival being more effectively blocked, compared to individual drug treatments (Fig. 6B, E). In addition, we find that upon inhibition of p38 MAPK and TNFα, the JNK pathway (74) is activated to promote apoptosis (Fig. 6E-F).Therefore, the combination of PFD and LY suppresses the inflammatory and stress response more effectively as it blocks upstream and downstream steps in the pathway to circumvent feedback reactivation or alternate pathways, which leads to the enhanced decrease in chemoresistant cell survival and cancer persistence *in vitro* and *in vivo* (Fig. 6, 7). These data indicate that blocking pro-inflammatory effectors—that are induced by chemotherapy mediated DNA damage and stress signaling—leads to increased chemosensitivity and decreased resistant cell survival.

EIF2α phosphorylation and mTOR inhibition reduces both rate limiting steps of canonical translation initiation (Fig. 2A-C). ATM and p38 MAPK can lead to activation of PKR and UPR stress-activated PERK, which phosphorylate eIF2α to decrease canonical tRNA recruitment and translation (Fig. 2B-C), leading to specific mRNA translation (33, 38, 42). These include cell cycle arrest factor, p27 KIP1(77) (Fig. S1C, S2A-B, p27), and GADD34 (Fig. S2H)—that are translated when canonical translation mechanisms are reduced (33, 42) as in G0 (13, 14). ATM activates AMPK which inhibits mTOR (17-19), leading to dephosphorylated, active 4EBP (Fig. 2B-C). 4EBP blocks canonical translation via eIF4E inhibition (35, 40), and permits non-canonical translation mechanisms of specific genes , including immune modulators like TNFα and CD47 (Fig. 2F-G, S2I, 3A-C, 5A-C,-D, S5A) (14), which activate survival genes (Fig. S5B).

Our findings revealed that these inflammatory genes upregulated in G0, have AREs and other UTR sequences that regulate mRNA levels and translation (Fig. 3A-C, S3A). The ATM-p38 MAPK-MK2 axis stabilize these ARE bearing pro-inflammatory cytokine mRNAs by phosphorylating ARE binding mRNA decay factor, TTP to prevent its mRNA decay activity on pro-inflammatory cytokine mRNAs like TNFα (Fig. 3D-K, 4A-B, 4F, 5A-C). This is consistent with previous studies on the role of AREs in cancers (14, 25, 28, 52, 54-56). All AML cell lines tested respond to the combination treatment that inhibits the p38 MAPK/MK2/TTP/TNFα axis leading to reduced TTP phosphorylation and inhibited TNFα (Fig. 6B, 6E-F) (28-30). These data suggest that the phospho-TTP and thus TTP activity, may be a key regulator of pro-inflammatory gene mediated chemoresistance. In support, overexpression of TTP-AA—that cannot be phosphorylated and is a dominant active form that restores ARE mRNA decay (28-30)—causes decrease in TNFα expression, and leads to reduced chemoresistance in both cell lines (Fig. 3G, 5C). These data suggest that phospho-TTP level is an important regulator of inflammatory response mediated chemoresistance, which can be harnessed as a marker and target against clinical resistance. Consistently, published in vivo leukemia resistance models show similar increased TTP and ARE bearing genes including inflammatory genes expressed (15, 78), as in our studies (Fig. 3A-F); additionally, inhibition of these pathways curtails chemoresistance *in vivo* in primary AML patients and tumor models (Fig. 7). Together, these pathways that are up-regulated in resistant cells (Fig. 4A, 5A) via chemotherapy and stress induced signaling—decrease canonical translation and permit non-canonical translation and post-transcriptional regulation of specific genes (Fig. S6)—to induce a pro-inflammatory response that promotes chemo-survival of G0 cancer cells.

Materials & Methods

Methods including details on plasmids, cell viability assays, flow cytometry, protein analysis, drugs, and motif analysis are described in Supplemental Information.

Cell Culture & Cell lines THP1 cells were cultured in Dulbecco's modified Eagle medium (RPMI)1460 media supplemented with 10% fetal bovine serum (FBS), 2 mM L-Glutamine, 100 μg/mL streptomycin and 100 U/ml penicillin at 37°C in 5% CO_2. SS THP1 cells were prepared by washing with PBS followed by serum-starvation at a density of 2×10^5 cells/mL and AraCS cells, by treatment with 5 μM AraC for 3 days or 9 days. MCF7, HFF, HEPG2 and U2OS cells were cultured in Dulbecco's modified Eagle medium (DMEM) media with 10% FBS, 2 mM L-Glutamine, 100 μg/mL streptomycin and 100 U/ml penicillin, as done previously (13, 14). MCF7 cells were serum-starved or treated with 150 uM Doxorubicin. THP1 (TIB-202), MV4:11 (CRL-9591), K562 (CCL243), HFF (SCRC-1041), MCF7 (HTB-22), U2OS (HTB-96) and HEPG2 (HB-8065) were obtained from ATCC. MOLM13 (ACC554), NOMO1 (ACC542) and MONOMAC6 (ACC124) were obtained from DSMZ. Cell lines kindly provided by David Scadden (79) and MOLM13-GFP-Luc by Monica Guzman (80) were tested for Mycoplasma (Promega) and authenticated by the ATCC Cell Authentication Testing Service (79).

Primary AML patient samples and human monocytes All human samples (de-identified) were handled in accordance with IRB protocols to SV (2015P000998/MGH), approved by the Partners Human Research Committee Institutional Review Board /MGH IRB, to DAS, and to TG (DF/HCC 13-583), approved by DF/HCC Office for Human Research Studies. AML samples used in this study were obtained by DAS including: MGH15 - bone marrow 60% blasts, karyotype 46, XX, t(9;11)(p22;q23)[20/20]; MGH22 - peripheral blood, 60% blasts, karyotype

46,XX,t(3;21)(q26;q22),t(9;22)(q34;q11.2)[18]/46,XX[2]; and MGH25 - bone marrow, 90% blasts, karyotype 46,XX[20] and by JL-S and TG including bone marrow samples: EQ1899, CI2095, PO2038, LA2053, NC1866, GO1122, CM2164, MV2192, VD2160, XD2101, VL2317, and OA2500. Bone marrow or peripheral blood mononuclear cells were isolated from de novo AML patients by ficoll density gradient centrifugation and cryopreserved with DMSO in a liquid nitrogen tank. Thawed cells were maintained in RPMI media with 10% FBS for several days before drugs treatment and analyses. Human CD34+ monocytes (2M-101) were obtained from Lonza. Primary cells from MLL-AF9, HoxA9-Meis1 mouse models were provided by DS (3). Mouse primary cells were maintained in RPMI media with 10% FBS, 2 mM L-Glutamine, 100 μg/mL streptomycin, 100 U/ml penicillin, 5 ng/ml murine IL-3 and 25 ng/ml murine Stem Cell Factor (SCF).

In vivo AML mouse models AML mouse models have been shown to predict therapy response accurately (81). C57BL/6 and NSG were obtained from MGH Cox-7 Gnotobiotic animal facility of the AAALAC-accredited Center for Comparative Medicine and Services at MGH. C57BL/6 or NSG mice were injected intravenously or subcutaneously with HoxA9-Meis1 or MOLM13 cells expressing luciferase (80, 82). IVIS imaging system (Perkin Elmer) were used to confirm engraftment of AML cells. Mice were intraperitoneally injected with 200 μl of luciferase substrate D-Luciferin (15 mg/ml) and anesthetized. Images were taken 5 or 10 minutes after D-Luciferin injection. After confirmation of engraftment by IVIS imaging, mice were randomly assigned to two groups and treated with pirfenidone (100 mg/kg, intraperitoneally), LY2228820 (20 mg/kg, intraperitoneally), AraC (30 mg/kg, intraperitoneally) or saline according at indicated combinations and dosages. Tumor volumes were measured by IVIS imaging at indicated time points.

Polysome profiling with microarray Sucrose was dissolved in lysis buffer containing 100 mM KCl, 5 mM $MgCl_2$, 100 μg/ml cycloheximide, 2 mM DTT and 10 mM Tris-HCl (pH 7.4). Sucrose gradients from 15% to 50% were prepared in ultracentrifuge tubes (Beckman) as previously described (13, 83-85). Cells were treated with 100 μg/mL cycloheximide at 37°C for 5 minutes before collecting them. Harvested cell were rinsed with ice-cold PBS having 100 μg/mL cycloheximide and then were resuspended in lysis buffer with 1% Triton X-100 and 40 U/mL murine (New England Biolabs) for 20 minutes. After centrifugation of cell lysates at 12,000 x g for 20 minutes, supernatants were loaded onto sucrose gradients followed by ultracentrifugation (Beckman Coulter Optima L90) at 34,000 × rpm at 4 °C for 2 hours in the SW40 rotor. Samples were separated by density gradient fractionation system (Teledyne Isco). RNAs were purified by using TRIzol (Invitrogen) from heavy polysome fractions and whole cell lysates. The synthesized cDNA probes from WT Expression Kit (Ambion) were hybridized to Gene Chip Human Transcriptome Array 2.0 (Affymetrix) and analyzed by the Partners Healthcare Center for Personalized Genetic Medicine Microarray and BUMC facilities. Gene ontology analysis for differentially expressed translatome or proteome was conducted by DAVID 6.7 tools (86) (87). Molecular signatures enriched in AraCS or SS were identified by Gene Set Enrichment Analysis (GSEA) (88).

Data Availability Raw datasets will be submitted to GEO public repository at final submission and will be available publicly as well as on request to the authors. TBD GEO accession number.

Statistical analyses & data availability are described in Supplemental Information.

Statement on Human Data All human samples (de-identified) were handled in accordance with IRB protocols to SV (2015P000998/MGH), approved by the Partners Human Research Committee

Institutional Review Board /MGH IRB, to DAS, and to TG (DF/HCC 13-583), approved by DF/HCC Office for Human Research Studies. Details in Supplemental Information.

Statement on animal data nod-scid-gamma (NSG), C57Black/6 mice, 10-12 weeks, are obtained from MGH Cox-7 Gnotobiotic animal facility of the AAALAC-accredited Center for Comparative Medicine and Services at MGH. These facilities are supervised by veterinarians in the Center for Comparative Medicine and the MGH Subcommittee for Animal Research (SRAC) and maintained according to the protocol approved by SRAC, and provide services for breeding, regular health checks, histopathology and macropathology.

Acknowledgments

We thank Partners Healthcare Center for Personalized Genetic Medicine & BUMC facilities for microarray data; N. Kedersha, S. Lyons & P. Anderson for plasmids & antibody; T. Graubert for patient samples; D. Bloch, S. Wu, A. Naar, M. Guzman, N. Bardeesy, D. Scadden, S. Ramaswamy, & C. Benes for reagents.

Author Contributions

SL conducted the research and bioinformatic analysis; SST, SIAB & DL contributed data; SL, YK, DM, BTN, ID-G, DTM, M-KC, DS, SM, & DAH provided in vivo models & in vivo data; MAM, RR & RG did immune data; AL, NJH, & ML provided mRNA folding energies & patient gene signatures; MB & WH conducted proteomics; DAS & JL-S provided patient samples; SV supervised the project & wrote the manuscript.

List of Supplemental files:

1. **Supplemental Information**

   Methods (related to main text, main figures 1-7 & supplemental figures S1-S6)

   Supplemental References (related to supplemental information, methods section)

   Supplemental Figure legends S1-S6, related to main figures 1-7

2. **Supplemental Figures S1-S6 (related to main figures 1-7)**

3. **Supplemental Tables 1-2 (related to main figures 1-7 & supplemental Figures S1-S6)**

Reference List

(1) Coller HA, Sang L, Roberts JM. A new description of cellular quiescence. PLoS Biol 2006;4:e83.

(2) Ng SW, Mitchell A, Kennedy JA, Chen WC, McLeod J, Ibrahimova N, et al. A 17-gene stemness score for rapid determination of risk in acute leukaemia. Nature 2016;540:433-7.

(3) Meacham CE, Morrison SJ. Tumor heterogeneity and cancer cell plasticity. Nature 2013;501:328-37.

(4) Crews LA, Jamieson CH. Selective elimination of leukemia stem cells: hitting a moving target. Cancer Lett 2013;338:15-22.

(5) Bhola PD, Mar BG, Lindsley RC, Ryan JA, Hogdal LJ, Vo TT, et al. Functionally identifiable apoptosis-insensitive subpopulations determine chemoresistance in acute myeloid leukemia. J Clin Invest 2016;126:3827-36.

(6) Tavaluc RT, Hart LS, Dicker DT, El-Deiry WS. Effects of low confluency, serum starvation and hypoxia on the side population of cancer cell lines. Cell Cycle 2007;6:2554-62.

(7) Gupta PB, Onder TT, Jiang G, Tao K, Kuperwasser C, Weinberg RA, et al. Identification of selective inhibitors of cancer stem cells by high-throughput screening. Cell 2009;138:645-59.

(8) Salony, Sole X, Alves CP, Dey-Guha I, Ritsma L, Boukhali M, et al. AKT Inhibition Promotes Nonautonomous Cancer Cell Survival. Mol Cancer Ther 2016;15:142-53.

(9) Li L, Bhatia R. Stem cell quiescence. Clin Cancer Res 2011;17:4936-41.

(10) Giles FJ, DeAngelo DJ, Baccarani M, Deininger M, Guilhot F, Hughes T, et al. Optimizing outcomes for patients with advanced disease in chronic myelogenous leukemia. Semin Oncol 2008;35:S1-17.

(11) Liu H, Adler AS, Segal E, Chang HY. A Transcriptional Program Mediating Entry into Cellular Quiescence. PLoS Genet 2007;3:e91.

(12) Sandberg R, Neilson JR, Sarma A, Sharp PA, Burge CB. Proliferating cells express mRNAs with shortened 3' untranslated regions and fewer microRNA target sites. Science 2008;320:1643-7.

(13) Lee S, Truesdell SS, Bukhari SI, Lee JH, Letonqueze O, Vasudevan S. Upregulation of eIF5B controls cell-cycle arrest and specific developmental stages. Proc Natl Acad Sci U S A 2014;111:E4315-E4322.

(14) Bukhari SI, Truesdell SS, Lee S, Kollu S, Classon A, Boukhali M, et al. A Specialized Mechanism of Translation Mediated by FXR1a-Associated MicroRNP in Cellular Quiescence. Mol Cell 2016;61:760-73.

(15) Ebinger S, Ozdemir EZ, Ziegenhain C, Tiedt S, Castro AC, Grunert M, et al. Characterization of Rare, Dormant, and Therapy-Resistant Cells in Acute Lymphoblastic Leukemia. Cancer Cell 2016;30:849-62.

(16) Saito Y, Kitamura H, Hijikata A, Tomizawa-Murasawa M, Tanaka S, Takagi S, et al. Identification of therapeutic targets for quiescent, chemotherapy-resistant human leukemia stem cells. Sci Transl Med 2010;2:17ra9.

(17) Shiloh Y, Ziv Y. The ATM protein kinase: regulating the cellular response to genotoxic stress, and more. Nat Rev Mol Cell Biol 2013;14:197-210.

(18) Tee AR, Proud CG. DNA-damaging agents cause inactivation of translational regulators linked to mTOR signalling. Oncogene 2000;19:3021-31.

(19) Jackson SP, Bartek J. The DNA-damage response in human biology and disease. Nature 2009;461:1071-8.

(20) Holohan C, Van Schaeybroeck S, Longley DB, Johnston PG. Cancer drug resistance: an evolving paradigm. Nat Rev Cancer 2013;13:714-26.

(21) Cuenda A, Rousseau S. p38 MAP-Kinases pathway regulation, function and role in human diseases. Biochimica et Biophysica Acta (BBA) - Molecular Cell Research 2007;1773:1358-75.

(22) Lalaoui N, Hanggi K, Brumatti G, Chau D, Nguyen NYN, Vasilikos L, et al. Targeting p38 or MK2 Enhances the Anti-Leukemic Activity of Smac-Mimetics. Cancer Cell 2016;29:145-58.

(23) Claudio N, Dalet A, Gatti E, Pierre P. Mapping the crossroads of immune activation and cellular stress response pathways. EMBO J 2013;32:1214-24.

(24) Senft D, Ronai ZA. UPR, autophagy, and mitochondria crosstalk underlies the ER stress response. Trends Biochem Sci 2015;40:141-8.

(25) Damgaard CK, Lykke-Andersen J. Regulation of ARE-mRNA Stability by Cellular Signaling: Implications for Human Cancer. Cancer Treat Res 2013;158:153-80.

(26) Cannell IG, Merrick KA, Morandell S, Zhu CQ, Braun CJ, Grant RA, et al. A Pleiotropic RNA-Binding Protein Controls Distinct Cell Cycle Checkpoints to Drive Resistance of p53-defective Tumors to Chemotherapy. Cancer Cell 2015;28:623-37.

(27) Brooks SA, Blackshear PJ. Tristetraprolin (TTP): interactions with mRNA and proteins, and current thoughts on mechanisms of action. Biochim Biophys Acta 2013;1829:666-79.

(28) Hitti E, Iakovleva T, Brook M, Deppenmeier S, Gruber AD, Radzioch D, et al. Mitogen-activated protein kinase-activated protein kinase 2 regulates tumor necrosis factor mRNA stability and translation mainly by altering tristetraprolin expression, stability, and binding to adenine/uridine-rich element. Mol Cell Biol 2006;26:2399-407.

(29) Tiedje C, Diaz-Munoz MD, Trulley P, Ahlfors H, Laaß K, Blackshear PJ, et al. The RNA-binding protein TTP is a global post-transcriptional regulator of feedback control in inflammation. Nucleic Acids Research 2016;44:7418-40.

(30) Clement SL, Scheckel C, Stoecklin G, Lykke-Andersen J. Phosphorylation of tristetraprolin by MK2 impairs AU-rich element mRNA decay by preventing deadenylase recruitment. Mol Cell Biol 2011;31:256-66.

(31) Forbes SA, Beare D, Gunasekaran P, Leung K, Bindal N, Boutselakis H, et al. COSMIC: exploring the world's knowledge of somatic mutations in human cancer. Nucleic Acids Res 2015;43:D805-D811.

(32) Loayza-Puch F, Drost J, Rooijers K, Lopes R, Elkon R, Agami R. p53 induces transcriptional and translational programs to suppress cell proliferation and growth. Genome Biol 2013;14:R32.

(33) Hsieh AC, Liu Y, Edlind MP, Ingolia NT, Janes MR, Sher A, et al. The translational landscape of mTOR signalling steers cancer initiation and metastasis. Nature 2012;485:55-61.

(34) Sendoel A, Dunn JG, Rodriguez EH, Naik S, Gomez NC, Hurwitz B, et al. Translation from unconventional 5' start sites drives tumour initiation. Nature 2017;541:494-9.

(35) Holcik M, Sonenberg N. Translational control in stress and apoptosis. Nat Rev Mol Cell Biol 2005;6:318-27.

(36) Zeenko VV, Wang C, Majumder M, Komar AA, Snider MD, Merrick WC, et al. An efficient in vitro translation system from mammalian cells lacking the translational inhibition caused by eIF2 phosphorylation. RNA 2008;14:593-602.

(37) Lorsch JR, Dever TE. Molecular view of 43 S complex formation and start site selection in eukaryotic translation initiation. J Biol Chem 2010;285:21203-7.

(38) Ron D, Walter P. Signal integration in the endoplasmic reticulum unfolded protein response. Nat Rev Mol Cell Biol 2007;8:519-29.

(39) Zismanov V, Chichkov V, Colangelo V, Jamet S, Wang S, Syme A, et al. Phosphorylation of eIF2alpha; Is a Translational Control Mechanism Regulating Muscle Stem Cell Quiescence and Self-Renewal. Cell Stem Cell 2016;18:79-90.

(40) Thoreen CC, Chantranupong L, Keys HR, Wang T, Gray NS, Sabatini DM. A unifying model for mTORC1-mediated regulation of mRNA translation. Nature 2012;485:109-13.

(41) Culjkovic B, Topisirovic I, Borden KL. Controlling gene expression through RNA regulons: the role of the eukaryotic translation initiation factor eIF4E. Cell Cycle 2007;6:65-9.

(42) Han K, Jaimovich A, Dey G, Ruggero D, Meyuhas O, Sonenberg N, et al. Parallel measurement of dynamic changes in translation rates in single cells. Nat Methods 2014;11:86-93.

(43) Damgaard CK, Lykke-Andersen J. Translational coregulation of 5G TOP mRNAs by TIA-1 and TIAR. Genes Dev 2011;25:2057-68.

(44) Shukla SA, Rooney MS, Rajasagi M, Tiao G, Dixon PM, Lawrence MS, et al. Comprehensive analysis of cancer-associated somatic mutations in class I HLA genes. Nat Biotechnol 2015;33:1152-8.

(45) Sosale NG, Spinler KR, Alvey C, Discher DE. Macrophage engulfment of a cell or nanoparticle is regulated by unavoidable opsonization, a species-specific 'Marker of Self' CD47, and target physical properties. Curr Opin Immunol 2015;35:107-12. doi: 10.1016/j.coi.2015.06.013. Epub;%2015 Jul 13.:107-12.

(46) Soto-Pantoja DR, Kaur S, Roberts DD. CD47 signaling pathways controlling cellular differentiation and responses to stress. Crit Rev Biochem Mol Biol 2015;50:212-30.

(47) Zhang H, Lu H, Xiang L, Bullen JW, Zhang C, Samanta D, et al. HIF-1 regulates CD47 expression in breast cancer cells to promote evasion of phagocytosis and maintenance of cancer stem cells. Proc Natl Acad Sci U S A 2015;112:E6215-E6223.

(48) de Kruijf EM, Sajet A, van Nes JG, Natanov R, Putter H, Smit VT, et al. HLA-E and HLA-G expression in classical HLA class I-negative tumors is of prognostic value for clinical outcome of early breast cancer patients. J Immunol 2010;185:7452-9.

(49) Majeti R, Chao MP, Alizadeh AA, Pang WW, Jaiswal S, Gibbs KD, et al. CD47 is an adverse prognostic factor and therapeutic antibody target on human acute myeloid leukemia stem cells. Cell 2009;138:286-99.

(50) Serrano M, Lin AW, McCurrach ME, Beach D, Lowe SW. Oncogenic ras provokes premature cell senescence associated with accumulation of p53 and p16INK4a. Cell 1997;88:593-602.

(51) Coppe JP, Desprez PY, Krtolica A, Campisi J. The senescence-associated secretory phenotype: the dark side of tumor suppression. Annu Rev Pathol 2010;5:99-118. doi: 10.1146/annurev-pathol-121808-102144.:99-118.

(52) Zhang T, Kruys V, Huez G, Gueydan C. AU-rich element-mediated translational control: complexity and multiple activities of trans-activating factors. Biochem Soc Trans 2001;30:952-8.

(53) Griseri P, Pages G. Control of pro-angiogenic cytokine mRNA half-life in cancer: the role of AU-rich elements and associated proteins. J Interferon Cytokine Res 2014;34:242-54.

(54) Nichols RC, Botson J, Wang XW, Hamilton BJ, Collins JE, Uribe V, et al. A flexible approach to studying post-transcriptional gene regulation in stably transfected mammalian cells. Mol Biotechnol 2011;48:210-7.

(55) Mukherjee N, Corcoran DL, Nusbaum JD, Reid DW, Georgiev S, Hafner M, et al. Integrative Regulatory Mapping Indicates that the RNA-Binding Protein HuR Couples Pre-mRNA Processing and mRNA Stability. Mol Cell 2011;43:327-39.

(56) Lal A, Mazan-Mamczarz K, Kawai T, Yang X, Martindale JL, Gorospe M. Concurrent versus individual binding of HuR and AUF1 to common labile target mRNAs. EMBO J 2004;23:3092-102.

(57) Moore AE, Chenette DM, Larkin LC, Schneider RJ. Physiological networks and disease functions of RNA-binding protein AUF1. Wiley Interdiscip Rev RNA 2014;5:549-64.

(58) White EJ, Brewer G, Wilson GM. Post-transcriptional control of gene expression by AUF1: mechanisms, physiological targets, and regulation. Biochim Biophys Acta 2013;1829:680-8.

(59) Zinder JC, Lima CD. Targeting RNA for processing or destruction by the eukaryotic RNA exosome and its cofactors. Genes Dev 2017;31:88-100.

(60) Gherzi R, Lee KY, Briata P, Wegmuller D, Moroni C, Karin M, et al. A KH domain RNA binding protein, KSRP, promotes ARE-directed mRNA turnover by recruiting the degradation machinery. Mol Cell 2004;14:571-83.

(61) Laroia G, Cuesta R, Brewer G, Schneider RJ. Control of mRNA decay by heat shock-ubiquitin-proteasome pathway. Science 1999;284:499-502.

(62) Sosa MS, Avivar-Valderas A, Bragado P, Wen HC, Aguirre-Ghiso JA. ERK1/2 and p38a/b Signaling in Tumor Cell Quiescence: Opportunities to Control Dormant Residual Disease. Clin Cancer Res 2011;17:5850-7.

(63) Patnaik A, Haluska P, Tolcher AW, Erlichman C, Papadopoulos KP, Lensing JL, et al. A First-in-Human Phase I Study of the Oral p38 MAPK Inhibitor, Ralimetinib (LY2228820 Dimesylate), in Patients with Advanced Cancer. Clin Cancer Res 2016;22:1095.

(64) Kuma Y, Sabio G, Bain J, Shpiro N, Marquez R, Cuenda A. BIRB796 inhibits all p38 MAPK isoforms in vitro and in vivo. J Biol Chem 2005;20;280:19472-9.

(65) Kagoya Y, Yoshimi A, Kataoka K, Nakagawa M, Kumano K, Arai S, et al. Positive feedback between NF-kappaB and TNF-alpha promotes leukemia-initiating cell capacity. J Clin Invest 2014;124:528-42.

(66) Frelin C, Imbert V, Griessinger E, Peyron AC, Rochet N, Philip P, et al. Targeting NF-kB activation via pharmacologic inhibition of IKK2-induced apoptosis of human acute myeloid leukemia cells. Blood 2005;105:804.

(67) Chang TP, Vancurova I. Bcl3 regulates pro-survival and pro-inflammatory gene expression in cutaneous T-cell lymphoma. Biochim Biophys Acta 2014;1843:2620-30.

(68) Haq R, Yokoyama S, Hawryluk EB, Jönsson GB, Frederick DT, McHenry K, et al. BCL2A1 is a lineage-specific antiapoptotic melanoma oncogene that confers resistance to BRAF inhibition. PNAS 2013;110:4321-6.

(69) Kurosu T, Fukuda T, Miki T, Miura O. BCL6 overexpression prevents increase in reactive oxygen species and inhibits apoptosis induced by chemotherapeutic reagents in B-cell lymphoma cells. Oncogene 2003;22:4459-68.

(70) Grattendick KJ, Nakashima JM, Feng L, Giri SN, Margolin SB. Effects of three anti-TNF-alpha drugs: etanercept, infliximab and pirfenidone on release of TNF-alpha in medium and TNF-alpha associated with the cell in vitro. Int Immunopharmacol 2008;8:679-87.

(71) Nakazato H, Oku H, Yamane S, Tsuruta Y, Suzuki R. A novel anti-fibrotic agent pirfenidone suppresses tumor necrosis factor-a at the translational level. European Journal of Pharmacology 2002;446:177-85.

(72) Rushworth SA, Bowles KM, Raninga P, MacEwan DJ. NF-kappaB-inhibited acute myeloid leukemia cells are rescued from apoptosis by heme oxygenase-1 induction. Cancer Res 2010;70:2973-83.

(73) Li ZW, Dalton WS. Tumor microenvironment and drug resistance in hematologic malignancies. Blood Reviews 2006;20:333-42.

(74) Liu J, Lin A. Role of JNK activation in apoptosis: A double-edged sword. Cell Research 2005;15:36.

(75) Townsend E, Murakami M, Christodoulou A, Christie A, K+¦ster J, Desouza T, et al. The Public Repository of Xenografts Enables Discovery and Randomized Phase II-like Trials in Mice. Cancer Cell30:183.

(76) Korb A, Tohidast-Akrad M, Cetin E, Axmann R, Smolen J, Schett G. Differential tissue expression and activation of p38 MAPK alpha, beta, gamma, and delta isoforms in rheumatoid arthritis. Arthritis & Rheumatism 2006;54:2745-56.

(77) Cuesta R, Martínez-Sánchez A, Gebauer F. miR-181a Regulates Cap-Dependent Translation of p27(kip1) mRNA in Myeloid Cells. Mol Cell Biol 2009;29:2841-51.

(78) Kesarwani M, Kincaid Z, Gomaa A, Huber E, Rohrabaugh S, Siddiqui Z, et al. Targeting c-FOS and DUSP1 abrogates intrinsic resistance to tyrosine-kinase inhibitor therapy in BCR-ABL-induced leukemia. Nature Medicine 2017;23:472.

(79) Sykes DB, Kfoury YS, Mercier FE, Wawer MJ, Law JM, Haynes MK, et al. Inhibition of Dihydroorotate Dehydrogenase Overcomes Differentiation Blockade in Acute Myeloid Leukemia. Cell 2016;167:171-86.

(80) Zong H, Gozman A, Caldas-Lopes E, Taldone T, Sturgill E, Brennan S, et al. A Hyperactive Signalosome in Acute Myeloid Leukemia Drives Addiction to a Tumor-Specific Hsp90 Species. Cell Rep 2015;13:2159-73.

(81) Zuber J, Radtke I, Pardee TS, Zhao Z, Rappaport AR, Luo W, et al. Mouse models of human AML accurately predict chemotherapy response. Genes Dev 2009;23:877-89.

(82) Chen Y, Jacamo R, Konopleva M, Garzon R, Croce C, Andreeff M. CXCR4 downregulation of let-7a drives chemoresistance in acute myeloid leukemia. J Clin Invest 2013;123:2395-407.

(83) Vasudevan S, Steitz JA. AU-rich-element-mediated upregulation of translation by FXR1 and Argonaute 2. Cell 2007;128:1105-18.

(84) Gandin V, Sikstrom K, Alain T, Morita M, McLaughlan S, Larsson O, et al. Polysome fractionation and analysis of mammalian translatomes on a genome-wide scale. J Vis Exp 2014;10.

(85) Truitt ML, Conn CS, Shi Z, Pang X, Tokuyasu T, Coady AM, et al. Differential Requirements for eIF4E Dose in Normal Development and Cancer. Cell 2015;162:59-71.

(86) Huang DW, Sherman BT, Lempicki RA. Systematic and integrative analysis of large gene lists using DAVID bioinformatics resources. Nat Protocols 2008;4:44-57.

(87) Huang DW, Sherman BT, Lempicki RA. Bioinformatics enrichment tools: paths toward the comprehensive functional analysis of large gene lists. Nucleic Acids Res 2009;37:1-13.

(88) Subramanian A, Tamayo P, Mootha VK, Mukherjee S, Ebert BL, Gillette MA, et al. Gene set enrichment analysis: A knowledge-based approach for interpreting genome-wide expression profiles. PNAS 2005;102:15545-50.

Figure legends

Figure 1. G0 leukemic cells induced by AraC or serum-starvation are chemoresistant and recapitulate gene expression programs of *in vivo* chemoresistant and G0 models. A. Transcriptome, translatome and proteome analyses in proliferating and G0 leukemic cells. G0 cells were induced by treatment of proliferating cells (S+) with 5 μM AraC or serum starved (SS). Total RNAs, polysome-associated mRNAs and protein were analyzed by comparative microarray and quantitative proteomics. **B.** Polysome profiles of S+, SS and AraC-surviving leukemic cells (AraCS) are shown. Heavy polysome-associated mRNAs were isolated and analyzed by microarray. **C**. Expression of Ki67 at the translatome level and flow cytometric quantification of G0/G1, S and G2/M phases, using BrdU and PI staining. **D**. Cell counting with trypan blue staining shows that SS or 5 μM AraC treatment on day 6 arrested cell proliferation reversibly. Cells resumed proliferation when serum was added to SS cells, or when AraCS cells were washed with PBS and resuspended in fresh media on day 11. **E**. Both AraCS and SS cells acquire resistance to AraC. S+, SS and AraCS cells were treated with various concentration of AraC for 3 days. Viable leukemic cells were measured by cell counting using trypan blue staining and IC_{50} values of AraC are shown. **F**. Comparison of transcriptomic, translatomic and proteomic changes in response to SS and 5 μM AraC treatments. **G**. Comparison of AraCS and SS with leukemic stem cells (LSC) (16) in AML, dormant leukemic cells (LRC) (15), minimal residual disease (MRD) (15) in ALL, and G0 fibroblasts (1). GSEA analysis was performed to determine whether previously published transcriptome signatures of LSC, LRC, MRD and G0 HFF are up-regulated in AraCS and SS cells, compared to S+ cells. 'N' marks the limited resolution of the proteome in the GSEA. $*P \leq 0.05$. Data are represented as average ± SEM. See also Fig. S1 & Table S1.

Figure 2. Inflammatory response mRNAs are selectively translated in G0 leukemic cells, where canonical translation is inhibited. A. Altered mechanisms of translation with repression of canonical translation. **B**. Polysome to monosome ratios in S+, SS and AraCS. **C**. Western analysis of translation initiation factor, eIF2α, and regulators eIF4EBP, PERK and PKR, in S+, SS and AraCS cells. **D**. Boxplot of the transcriptome and translatome changes in known TOP mRNAs in response to SS or AraC treatment. **E.** Number of differentially expressed genes. **F.** Venn diagram shows 162 genes up-regulated at both the transcriptome and translatome levels and 180 genes translationally up-regulated, where ribosome occupancy, RO increases by 1.5-fold. Heatmap shows gene expression changes in RNA, translatome levels and RO. **G.** Gene ontology (GO) analyses of differentially expressed genes. Statistical significance of enriched GO categories is shown as a heatmap. **H**. GSEA was performed to determine whether gene signatures of G0 leukemic cells is conserved in other G0 cells. **I**. GSEA shows gene categories regulated commonly in the translatome of G0 cells from five different cell types. Heatmap of normalized enrichment score (NES) is shown. $*P \leq 0.05$. Data are represented as average ± SEM. See also Fig. S2 & Table S1.

Figure 3. Phosphorylation of TTP by p38 MAPK/MK2 up-regulates ARE-bearing mRNAs in G0 leukemic cells. A. Boxplot of ARE scores (SI methods) in the 3′UTRs of genes, up- or down-regulated at the translatome level in G0 compared to S+ cells. **B**. Venn diagram shows genes that are up-regulated at the translatome level and have AREs in their 3′UTRs (left). List of such genes (right). **C**. Expression of indicated ARE genes at the RNA and translatome levels. **D.** Western analysis of TNFα. **E.** Scatter plot showing the expression of RNA binding protein genes from RBPDB database (SI methods). TTP is indicated with a green dot. **F.** Western analysis of TTP in lysates from S+, SS and AraCS cells in the absence or presence of alkaline phosphatase (AP). Phospho-TTP is indicated with an arrow. **G.** Bar

graph shows TNFα mRNA expression normalized to GAPDH mRNA upon over-expression of vector or c-myc tagged non-phosphorylatable mutant TTP (TTP-AA) in AraC-treated THP1 or K562 cells. Western analysis of TTP-AA with c-myc antibody (right). **H**. Activation of p38 MAPK/MK2 permits stabilization and translation of ARE-bearing mRNAs via TTP phosphorylation in chemoresistant G0 cells. LY2228820 (LY) and BIRB396 (BIRB) are p38 MAPK inhibitors. Western analysis of indicated proteins in lysates from THP1 cells **I**. at indicated time points after AraC treatment, and **J**. in S+ and AraCS cells treated with vehicle, 5 μM LY or 5 μM BIRB. **K**. Bar graph shows Firefly luciferase activity of a reporter bearing TNFα ARE in its 3′UTR normalized to activity of co-transfected Renilla luciferase in S+ and AraCS cells treated with vehicle, 5 μM LY. $*P \leq 0.05$. Data are represented as average ± SEM. See also Fig. S3 & Table S2.

Figure 4. Targeting p38 MAPK/MK2 signaling that is transiently activated in early G0, reduces AraC resistance. **A**. Western analysis of indicated proteins in THP1 cells at time points after serum starvation or 5 μM AraC treatment. **B**. Ratio of phospho-p38 MAPK, phospho-MK2 or TTP to p38 MAPK, MK2 or tubulin (loading control), respectively. **C**. Sequential treatment with p38 MAPK inhibitors and AraC in leukemic cells. **D & E**. Effects of p38 MAPK/MK2 inhibitions on survival of AraC-resistant cells. THP1 cells were treated with 5 μM BIRB796 (BB), 5 μM LY and vehicle in the absence (top panels, S+) or presence (bottom panels, AraC) of 5 μM AraC treatment for three days. Bar graphs show relative cell viability and death assessed by cell counting, MTS and caspase 3/7 assays. In the presence of AraC, THP1 cells were treated with p38 MAPK inhibitors prior to AraC treatment (BB → AraC, LY → AraC), at the same time with AraC (AraC + BB) and 1 day after AraC (AraC → BB, AraC → LY). 'H' and 'D' indicate hour(s) and day(s), respectively. **F**. Effect of p38 MAPK/MK2 inhibition on survival of resistant cells from five AML cell lines (M5 FAB subtype). Cells were treated

with 5 μM LY or vehicle 4 hours prior to AraC treatment (top panel, AraC) or in the absence of AraC (bottom panel, S+). Human CD34+ cells from healthy donors were tested as a control. **G**. Effect of p38 MAPK/MK2 inhibition on survival of chemoresistant cells with various concentrations of AraC. MV4:11 leukemic cells were treated with 5 μM LY or vehicle prior to 0 μM, 0.2 μM, 0.5 μM or 1 μM AraC for 3 days. *$P \leq 0.05$. Data are represented as average ± SEM. See also Fig. S4.

Figure 5. Targeting TTP-TNFα and downstream NF-kB signaling sensitizes resistant leukemic cells to AraC treatment. **A**. Phosphorylation of TTP by p38 MAPK/MK2 stabilizes ARE-bearing TNFα mRNA, resulting in activation of NF-kB signaling in resistant G0 leukemic cells. TNFα expression is inhibited by TTP-AA mutant, pirfenidone (PFD) or shRNAs, and NF-kB signaling by NF-kB inhibitor, Bay11-7082. **B**. Expression of TNFα and NF-kB target genes at the translatome level at indicated time points after SS or AraC treatment. **C**. TTP-AA mutant expression prior to 5 μM AraC treatment, depleted TNFα in THP1 or K562 cells as shown in Fig. 3G. Viability of cells with TTP-AA or control vector was assessed by cell count. **D**. Cell viability (left) and Western analysis of TNFα (right) in stable THP1 cell lines expressing doxycycline-inducible shRNA against TNFα or control shRNA, which were treated with doxycycline, recombinant TNFα (ReTNFα) or 5 μM AraC. Recombinant TNFα protein was added 1 day prior to AraC (ReTNFα → AraC) and shRNA against TNFα was induced prior to AraC (shTNFα → AraC) or after AraC (AraC → shTNFα). **E**. Sequential treatment with PFD and AraC (left). TNFα expression at the translatome (middle) and protein levels (right) in response to PFD treatment. **F**. Effect of pharmacological inhibition of TNFα by PFD on AraC resistance. THP1 cells were treated with 300 μg/ml PFD or vehicle in the absence of AraC (S+, top panel), in the presence of AraC (AraC, middle panel), or on serum starvation (SS, bottom panel). Bar graphs show cell viability and death assessed by cell counting, MTS and caspase 3/7 assays. In middle

or bottom panels, THP1 cells were treated with PFD 1 day prior to AraC or SS (PFD → AraC, PFD → SS), at the same time with AraC or SS (AraC + PFD, SS + PFD), and 1 day after AraC or SS (AraC → PFD, SS → PFD). **G**. Effect of TNFα inhibition on AraC resistance from six different leukemic cell lines. Cells were treated with PFD or vehicle 1 day prior to AraC (top panel, AraC) or in the absence of AraC (bottom panel, S+). **H**. Effect of NF-kB inhibition on AraC resistance. THP1 cells were treated with 10 μM Bay11-7082 or vehicle in the absence of AraC (S+, top panel), in the presence of AraC (AraC, middle panel) or under serum starvation (SS, bottom panel). In middle or bottom panels, THP1 cells were treated with Bay11-7082 1 day prior to AraC or SS (Bay → AraC, Bay → SS), at the same time with AraC or SS (AraC + Bay, SS + Bay), and 1 day after AraC or SS (AraC → Bay, SS → Bay). *$P \leq 0.05$. Data are represented as average ± SEM. See also Fig. S5.

Figure 6. PLA combination therapy decreases AraC-resistant cells by reducing TNFα and activating pro-apoptotic JNK pathway. A. PLA therapy, involves pre-treatment of leukemic cells with PFD and LY for 1 day and 4 hours, respectively, followed by AraC treatment, using half of the concentrations used for individual drugs in Fig. 4 and 5. **B**. Three different AML cell lines were sequentially treated with indicated drugs, followed by assessment of cell viability and death. **C**. Ratio of apoptotic to living MOLM13 cells treated with indicated drug combinations (left). Flow cytometric profiles of cells stained with annexin V and propidium iodide (right). **D**. Quantification of colonies in MOLM13 cells treated with indicated drug combinations and then plated on methylcellulose media (left). Colony images are shown (right). **E.** Western analyses of indicated proteins in THP1 and MOLM13 cells treated with indicated drugs. Phospho-TTP is indicated with an arrow. **F**. Rescue of MOLM13 cells from PLA therapy-mediated apoptosis by inhibition of JNK pathway with JNK-IN-8.

Cell viability and death (left) and Western analyses of phospho-JNK, phospho-c-Jun and c-Jun (right) are shown $*P \leq 0.05$. Data are represented as average ± SEM. See also Fig. S5.

Figure 7. PLA therapy significantly reduces AraC resistance in primary AML cells *ex vivo* and *in vivo*. A. Viability of primary cells from AML patients and normal CD34+ cells from healthy donors after indicated treatments. **B**. Viability and death of primary cells from AML mouse models driven by HoxA9-Meis1 and MLL-AF9 after indicated treatments. **C-G.** Bioluminescence images and quantification of tumor growth **C-D**. in NSG mice engrafted with MOLM13 cells and treated with PLA therapy or AraC, **E-F**. in C57BL/6 mice engrafted with primary HoxA9-Meis1/luciferase cells and treated with PLA therapy or AraC, and **G.** with PFD plus LY or vehicle as a control. Kaplan-Meier survival curves of mice with PLA therapy or AraC is shown below. $*P \leq 0.05$. Data are represented as average ± SEM. See also Fig. S6.

Figure 1

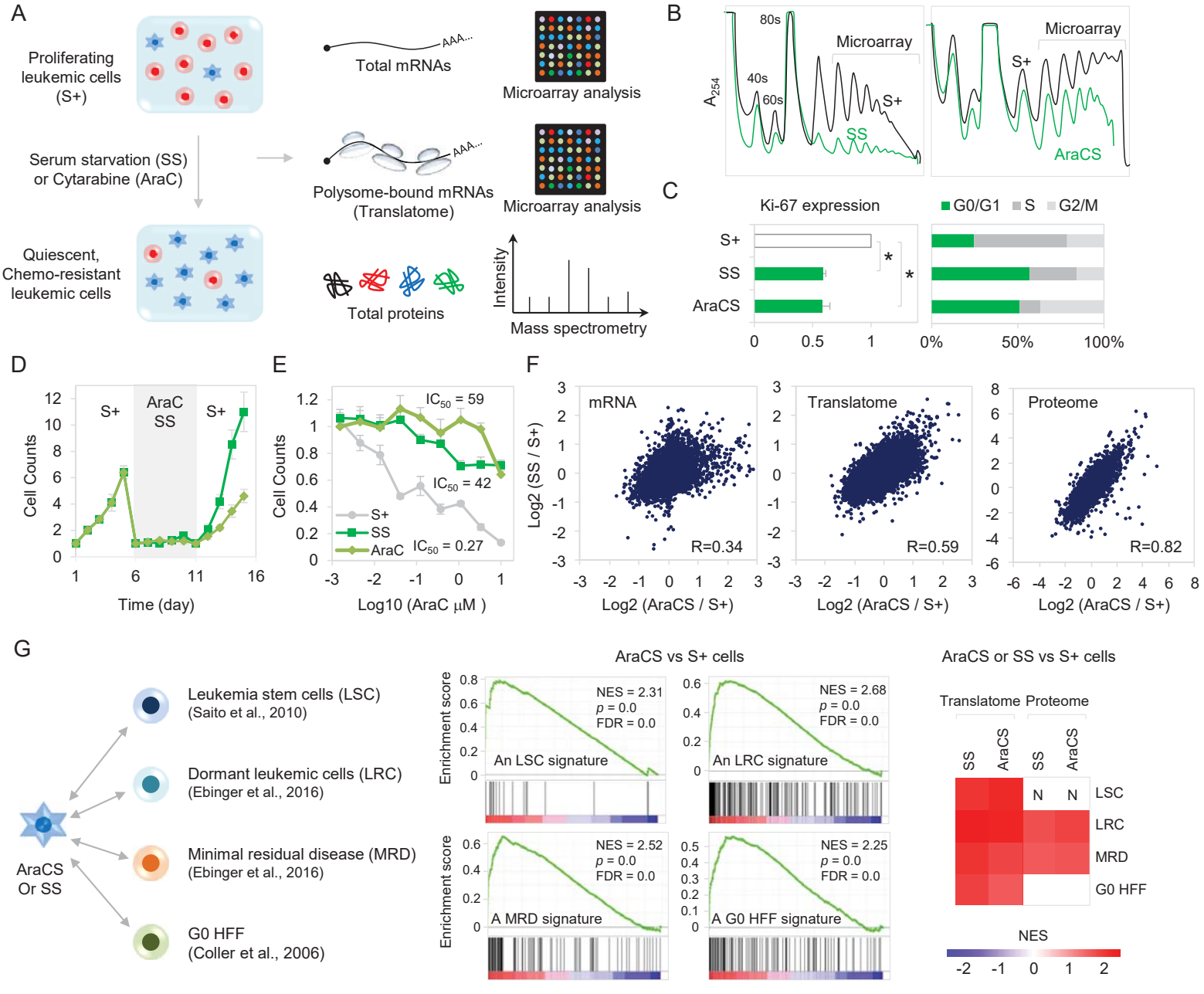

Figure 2

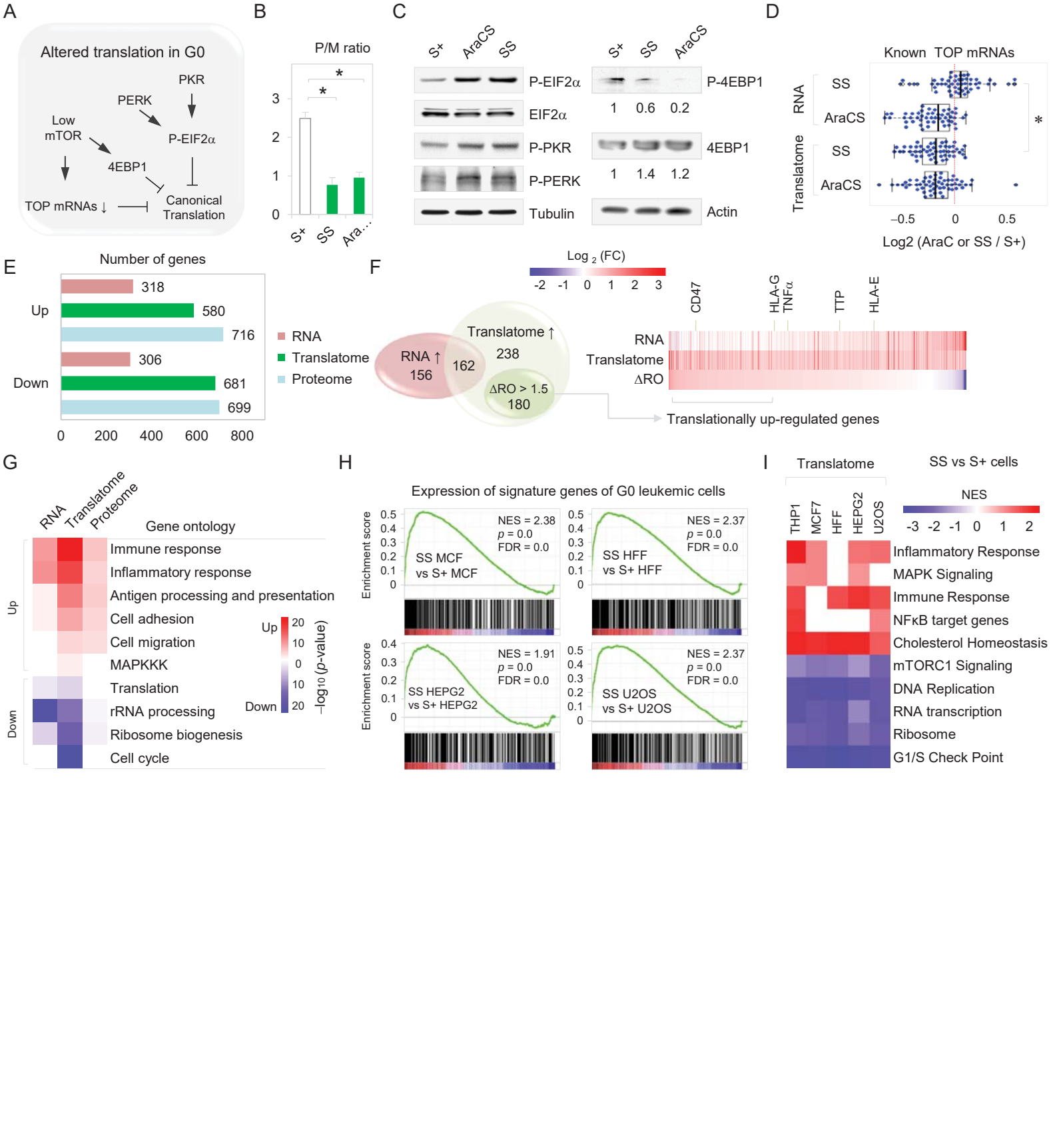

Figure 3

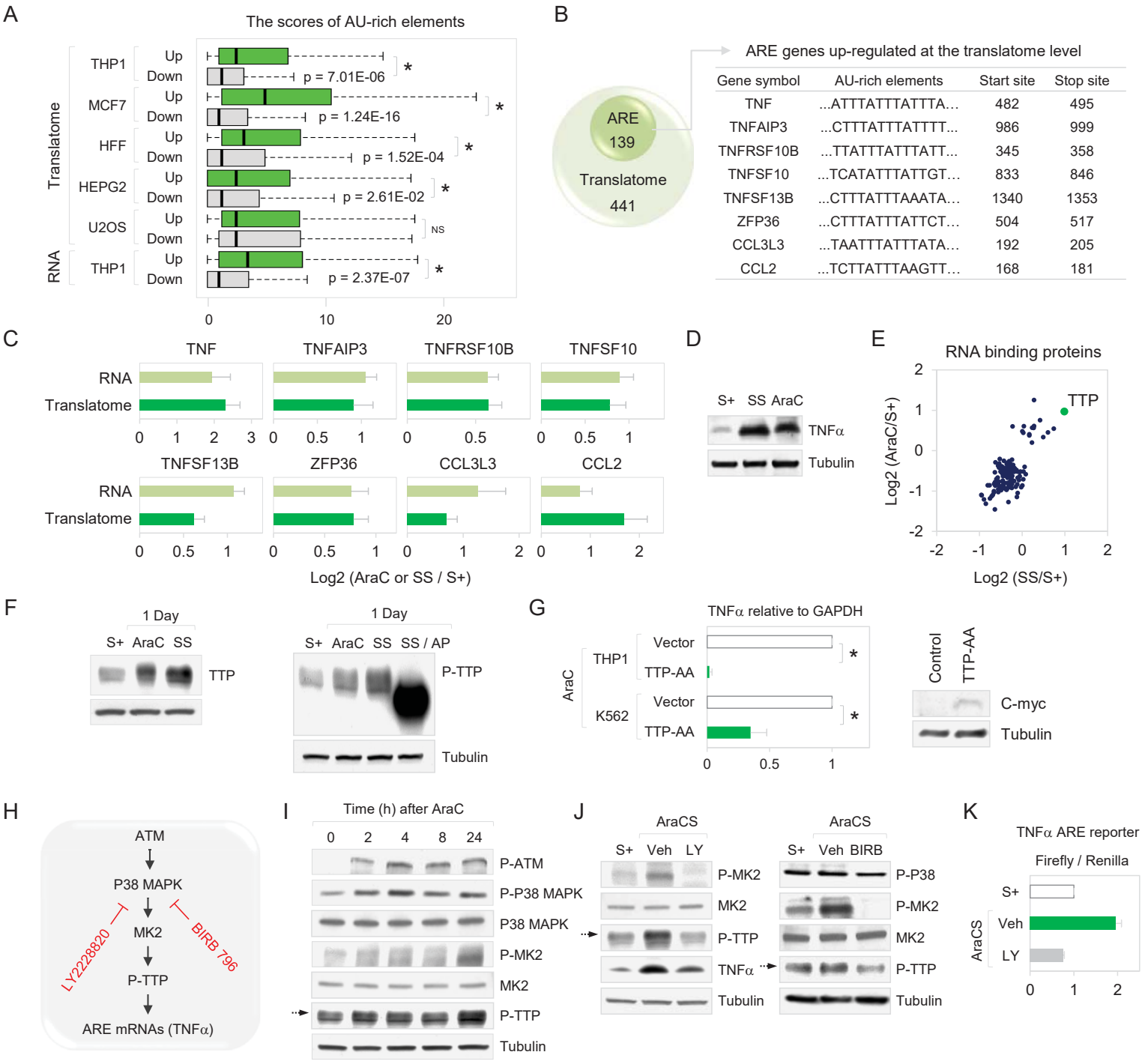

Figure 4

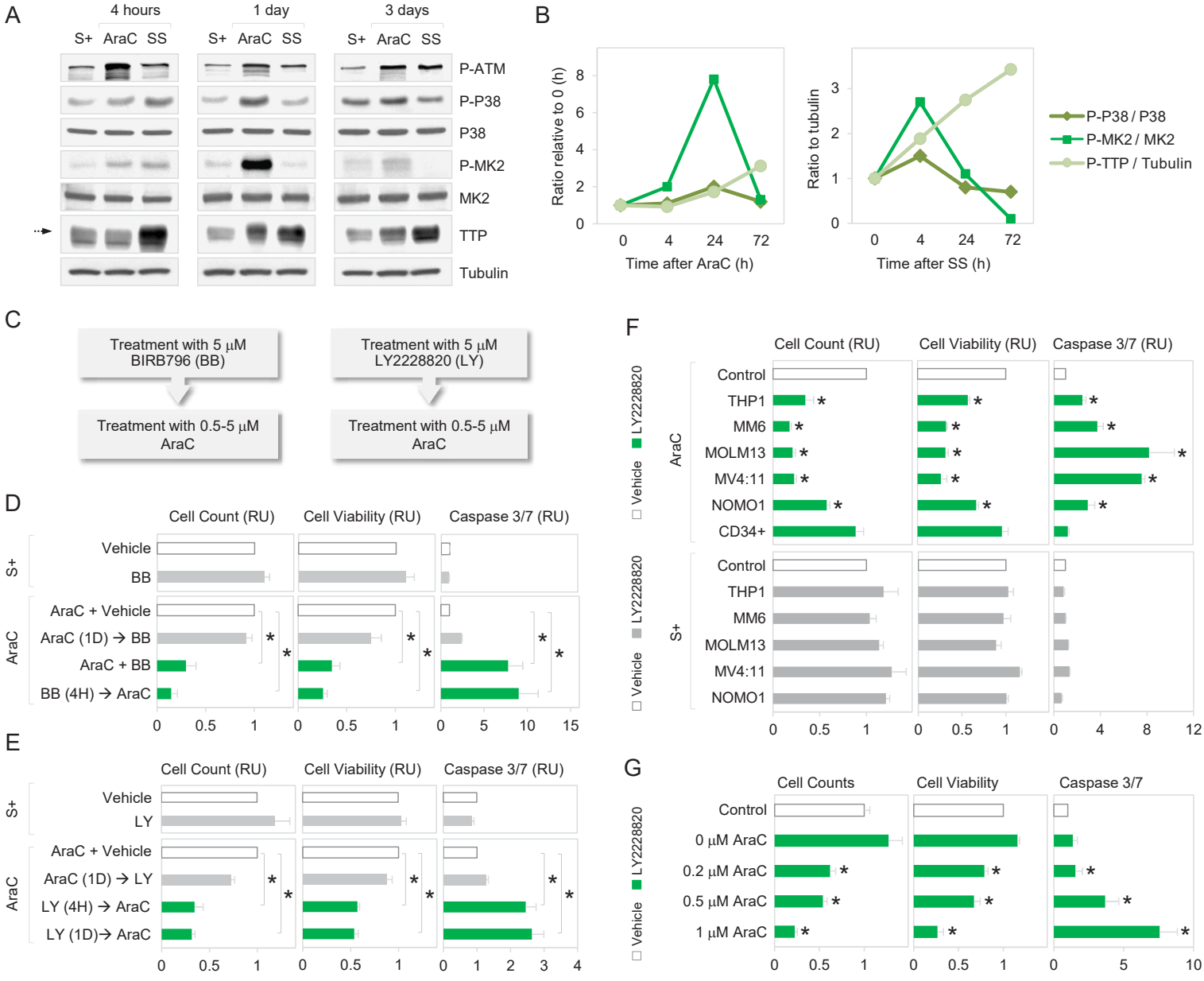

Figure 5

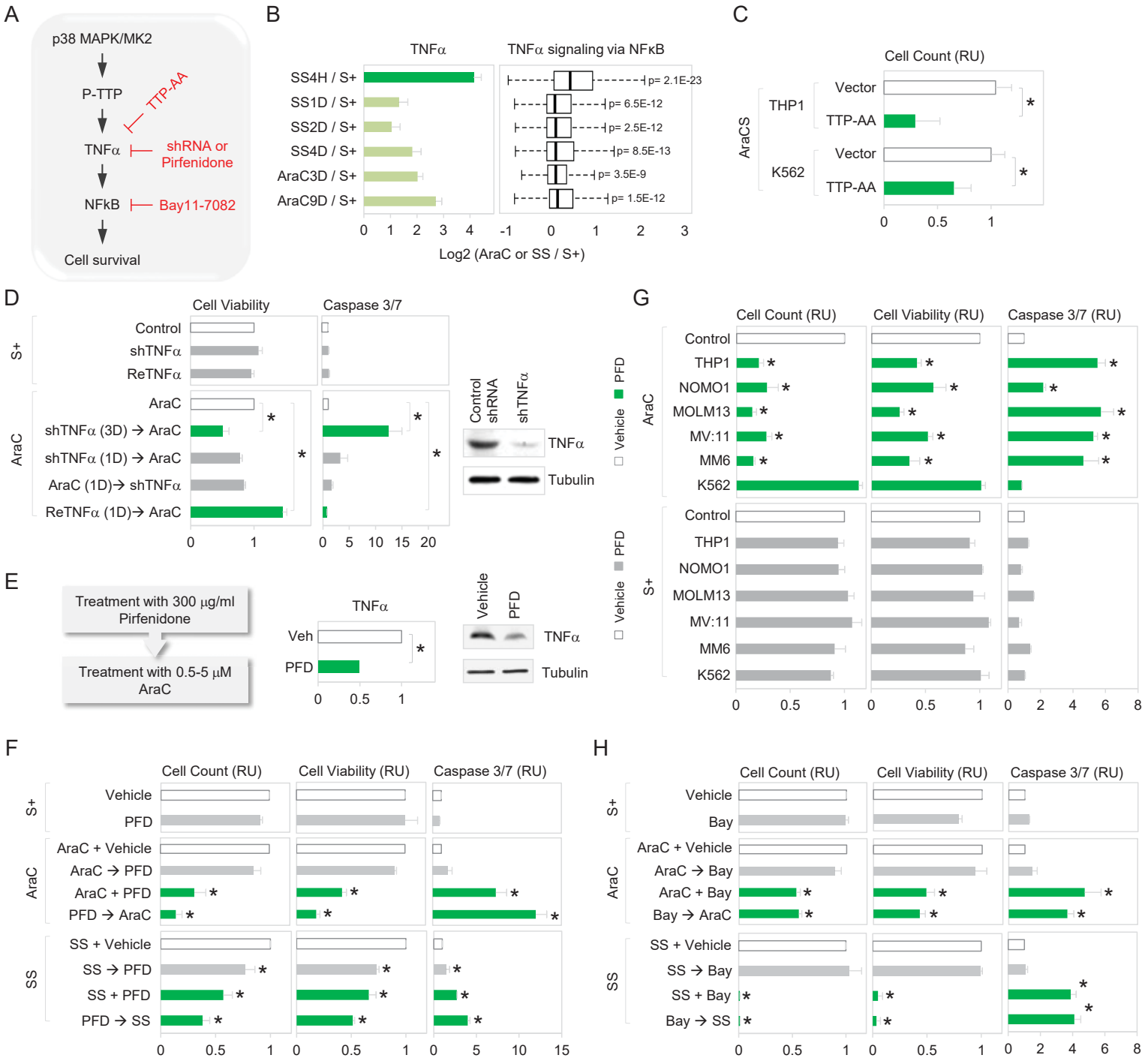

Figure 6

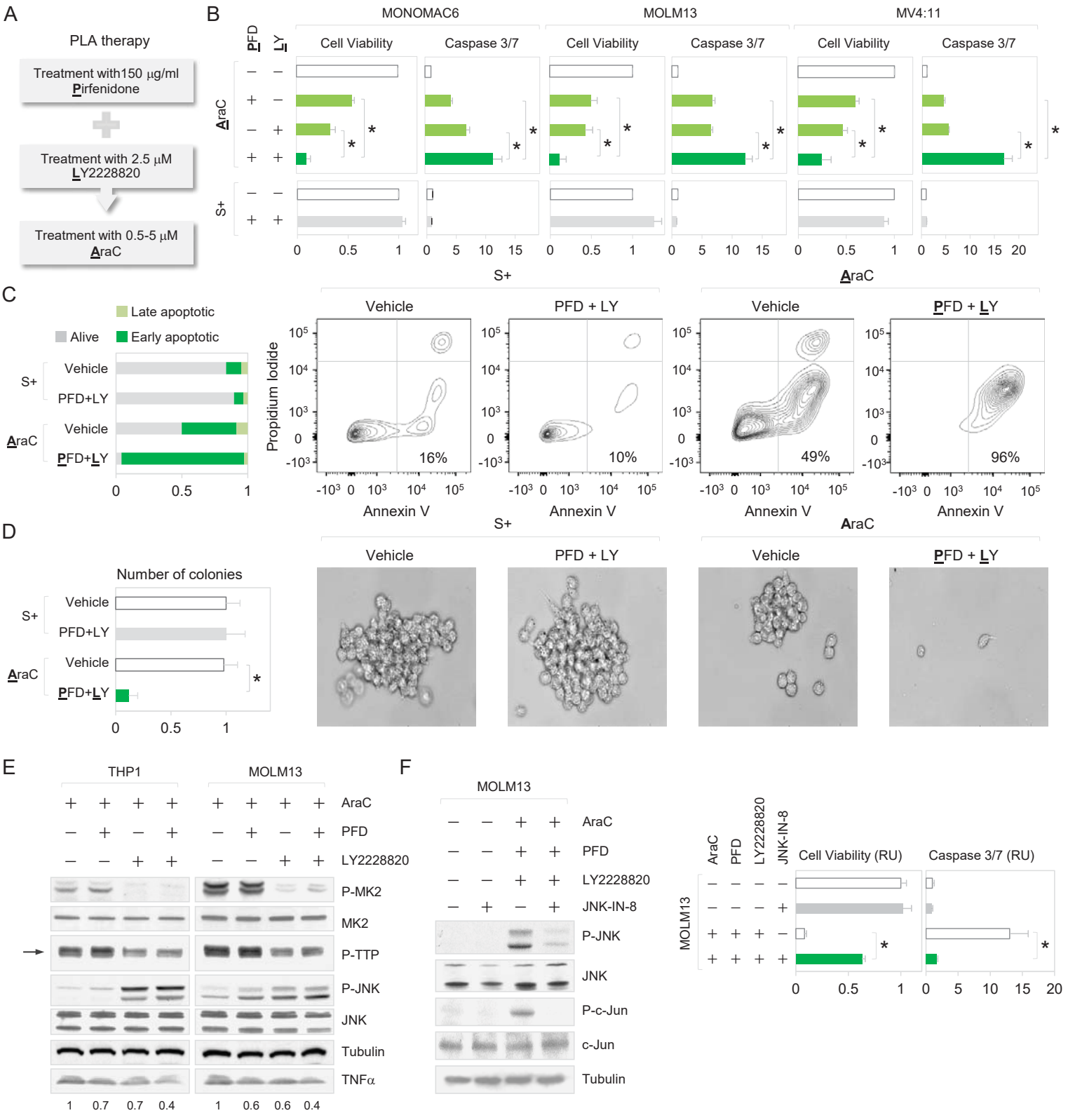

Figure 7

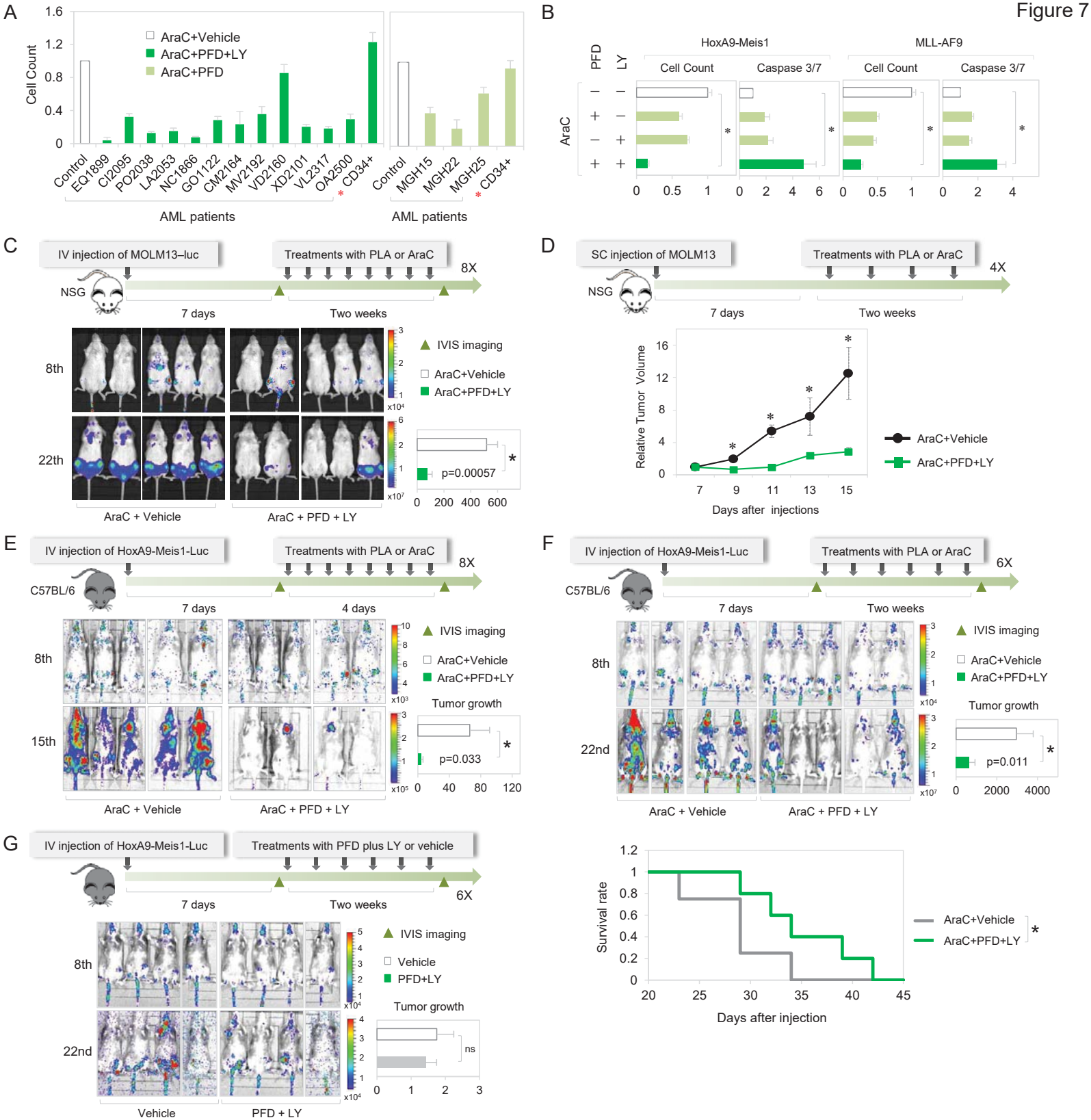

A post-transcriptional program of chemoresistance by AU-rich elements/TTP in cancer quiescence

List of Supplemental Information

Methods (related to main text, main figures 1-7 & supplemental figures S1-S6)

Plasmids

TRIPZ plasmids expressing shRNA against human TNFα (V2THS_111606), and miR30a primiR sequences used as control (RHS4750), were obtained from Open Biosystems and MGH cancer center, respectively. Stable cell lines were constructed as described by Open Biosystems. The stable cells expressing shRNA against TNFα were induced with 1 μg/mL doxycycline at indicated time points to knockdown TNFα. Luciferase reporters to test ARE expression were previously described (1). Cells were treated with 10 ng/ml recombinant TNFα (R&D Systems) to activate NFκB pathway. Myc-tagged TTP-AA (2, 3) was a gift from Nancy Kedersha and Shawn Lyons from Paul Anderson's lab.

MTS assay

MTS assay, a colorimetric quantification of viable cells was conducted as described by the manufacturer, Promega. A volume of 100 μl cells was placed in a 96-well plate after drugs treatment. A volume of 20 μl MTS reagent (CellTiter 96® Aqueous Non-Radioactive Cell Proliferation Assay) was added to each well followed by incubation at 37°C for 1 hour. Absorbance was measured at 490 nm by using a microplate reader.

Caspase 3/7 assay

After drugs treatment, cell death was measured by using caspase-glo® 3/7 assay kit (Promega) according to the protocol provided by the manufacturer. The equal volume of caspase-glo reagent was

added to cells, and samples were gently mixed with pipetting. The plates were incubated at room temperature in the dark for 2 hours. The luminescence of each sample was measured in a luminometer (Turner BioSystems).

Flow cytometry and cell cycle analysis

Cell proliferation was determined by flow cytometry of cells labeled with propidium iodide and bromodeoxyuridine (BrdU). The cells were incubated with 10 μM BrdU for 90 minutes at 37°C in 5% CO_2 before harvesting. Collected cells were fixed in ice cold 70% ethanol overnight. Cells were washed in PBS and treated with 2 M HCl for 30 min. Cells were incubated for 1 hour with anti-BrdU antibody conjugated to FITC (eBioscience) in the dark, washed and stained with propidium iodide. Samples were filtered through a nylon mesh filter and cell cycle analysis performed on the flow cytometry (4).

Western blot analysis

Cells were collected and resuspended in lysis buffer containing 40 mM Tris-HCl (pH 7.4), 6 mM $MgCl_2$, 150 mM NaCl, 0.1% NP-40, 1 mM DTT and protease inhibitors (Roche). Samples containing 80 μg of protein were loaded onto 10% or 12% SDS-PAGE (Bio-Rad), transferred to PVDF membranes and processed for immunoblotting. Antibodies against p27 (06-445) and tubulin (05-829) were obtained from Millipore. Antibodies against HES1 (sc-25392), eIF2α (sc-11386) and phospho-4EBP1 (sc-1809) were from Santacruz. Antibodies against phospho-ATM (ab81292), phospho-PKR (ab32036) and phospho-IRE1 (ab124945) were from Abcam. Antibodies against phospho-PERK (649401) were from Biolegend. Antibodies again TNFα (3707), phospho-p38 MAPK (4511), phospho-MK2 (3007), phospho-eIF2α (9721), TTP (71632) and 4EBP1 (9452) were from Cell Signaling Technology.

Apoptosis analysis

Leukemic cells were treated with indicated drug combinations. Annexin V FITC/PI staining was performed with FITC Annexin V Apoptosis Detection Kit I (BD Pharmingen). Flow cytometry analysis and FlowJo software were used to quantitate the percentages of apoptotic cells.

Colony forming assay

After treatment with indicated drug combinations, the same number of cells were plated in methylcellulose-based media with human recombinant cytokines (stem cell technology, MethoCult™ H4435). Number of colonies was quantitated in each plate after 10 days.

Mass Spectrometry

Multiplex quantitative proteomics analysis was conducted, as previously(5), from S+, SS and AraC treated THP1 leukemic cells.

Inhibitors

Pirfenidone (10 to 300 μg/ml (6-9)) was obtained from Chemietek. AraC (1 to 10 μM (10, 11)), LY2228820 (0.03 to 2 μM (12-15)), BIRB796 (BIRB, 5μM (16-20)), and JNK-IN-8(21) were from

Selleckchem. KU55933 (10 μM (22)), BAY 11-7082 (10 μM (23)) and D-luciferin were from Cayman Chemical and Doxorubicin (10 to 500 nM (24)) was from Tocris Bioscience.

Motif, AREs, RNA binding proteins & Ribosome occupancy analysis

The Multiple Em for Motif Elicitation (MEME) software was used to search for cis-elements enriched in 5' UTR of translationally regulated genes (25). Human 5' UTR sequences were retrieved from UCSC table browser (26). In a discriminative mode, 5' UTR sequences of translationally up- or down-regulated genes were used as the primary sequences and 5' UTR sequences of translationally unchanged genes, the control sequences. Motifs were found in the given strand with 6-30 nt motif width. We compared polysome-associated mRNAs with their total RNA levels in serum-starved and AraCS cells to generate the change in ribosome occupancy (RO)(27-29)—which is the ratio of the level of mRNA that is associated with heavy polysomes compared to the total mRNA level of each gene (Fig. 2F, venn diagram, heat map). ARE Score algorithm (30) was used to assess scores of AU-rich elements quantitatively. The list of RNA binding protein genes were obtained from RBPDB database (31).

Statistical analyses

All experiments in every figure used at least 3 biological replicates except for microarray, mass spectrometry, and patient sample data. Each experiment was repeated at least 3 times. No statistical method was used to pre-determine sample size. Sample sizes were estimated on the basis of availability and previous experiments (32, 33). No samples were excluded from analyses. P values and statistical tests were conducted for each figure. Statistical analyses were conducted using R or Excel. Two-tailed

unpaired t-test or Wilcoxon rank sum test was applied to assess statistical significance. SEM (standard error of mean) values are shown as error bars in all figures. Means were used as center values in box plots. P-values less than 0.05 were indicated with an asterisk. E-values were used for the statistical significance in the motif analysis.

Reference List

(1) Vasudevan S, Steitz JA. AU-rich-element-mediated upregulation of translation by FXR1 and Argonaute 2. Cell 2007;128:1105-18.

(2) Stoecklin G, Stubbs T, Kedersha N, Wax S, Rigby WF, Blackwell TK, et al. MK2-induced tristetraprolin:14-3-3 complexes prevent stress granule association and ARE-mRNA decay. EMBO J 2004;23:1313-24.

(3) Sun L, Stoecklin G, Van WS, Hinkovska-Galcheva V, Guo RF, Anderson P, et al. Tristetraprolin (TTP)-14-3-3 complex formation protects TTP from dephosphorylation by protein phosphatase 2a and stabilizes tumor necrosis factor-alpha mRNA. J Biol Chem 2007;282:3766-77.

(4) Hoy CA, Seamer LC, Schimke RT. Thermal denaturation of DNA for immunochemical staining of incorporated bromodeoxyuridine (BrdUrd): Critical factors that affect the amount of fluorescence and the shape of BrdUrd/DNA histogram. Cytometry 1989;10:718-25.

(5) Ting L, Rad R, Gygi SP, Haas W. MS3 eliminates ratio distortion in isobaric labeling-based multiplexed quantitative proteomics. Nat Methods 2011;8:937-40.

(6) Ozes O, Blatt LM, Seiwert SD. Use of pirfenidone in therapeutic regimens. United States Patent-US 7,407,973 . B2, 1-46. 8-5-2008.
Ref Type: Generic

(7) Schaefer CJ, Ruhrmund DW, Pan L, Seiwert SD, Kossen K. Antifibrotic activities of pirfenidone in animal models. European Respiratory Review 2011;20:85.

(8) King TE, Bradford WZ, Castro-Bernardini S, Fagan EA, Glaspole I, Glassberg MK, et al. A Phase 3 Trial of Pirfenidone in Patients with Idiopathic Pulmonary Fibrosis. N Engl J Med 2014;370:2083-92.

(9) Grattendick KJ, Nakashima JM, Feng L, Giri SN, Margolin SB. Effects of three anti-TNF-alpha drugs: etanercept, infliximab and pirfenidone on release of TNF-alpha in medium and TNF-alpha associated with the cell in vitro. Int Immunopharmacol 2008;8:679-87.

(10) Kojima K, Konopleva M, Samudio IJ, Shikami M, Cabreira-Hansen M, McQueen T, et al. MDM2 antagonists induce p53-dependent apoptosis in AML: implications for leukemia therapy. Blood 2005;106:3150-9.

(11) Grant S. Ara-C: Cellular and Molecular Pharmacology. In: George F, V, editor. Advances in Cancer Research. Volume 72 ed. Academic Press; 1997. p. 197-233.

(12) Tate C, Blosser W, Wyss L, Evans G, Xue Q, Pan Y, et al. LY2228820 Dimesylate, a Selective Inhibitor of p38 Mitogen-activated Protein Kinase, Reduces Angiogenic Endothelial Cord Formation in Vitro and in Vivo. Journal of Biological Chemistry 2013;288:6743-53.

(13) Campbell RM, Anderson BD, Brooks NA, Brooks HB, Chan EM, De DA, et al. Characterization of LY2228820 dimesylate, a potent and selective inhibitor of p38 MAPK with antitumor activity. Mol Cancer Ther 2014;13:364-74.

(14) Patnaik A, Haluska P, Tolcher AW, Erlichman C, Papadopoulos KP, Lensing JL, et al. A First-in-Human Phase I Study of the Oral p38 MAPK Inhibitor, Ralimetinib (LY2228820 Dimesylate), in Patients with Advanced Cancer. Clin Cancer Res 2016;22:1095.

(15) Lalaoui N, Hanggi K, Brumatti G, Chau D, Nguyen NYN, Vasilikos L, et al. Targeting p38 or MK2 Enhances the Anti-Leukemic Activity of Smac-Mimetics. Cancer Cell 2016;29:145-58.

(16) Pargellis C, Tong L, Churchill L, Cirillo PF, Gilmore T, Graham AG, et al. Inhibition of p38 MAP kinase by utilizing a novel allosteric binding site. Nat Struct Biol 2002;9:268-72.

(17) Yasui H, Hideshima T, Ikeda H, Jin J, Ocio EM, Kiziltepe T, et al. BIRB 796 enhances cytotoxicity triggered by bortezomib, heat shock protein (Hsp) 90 inhibitor, and dexamethasone via inhibition of p38 mitogen-activated protein kinase/Hsp27 pathway in multiple myeloma cell lines and inhibits paracrine tumour growth. Br J Haematol 2007;136:414-23.

(18) Regan J, Breitfelder S, Cirillo P, Gilmore T, Graham AG, Hickey E, et al. Pyrazole urea-based inhibitors of p38 MAP kinase: from lead compound to clinical candidate. J Med Chem 2002;45:2994-3008.

(19) Kuma Y, Sabio G, Bain J, Shpiro N, Marquez R, Cuenda A. BIRB796 inhibits all p38 MAPK isoforms in vitro and in vivo. J Biol Chem 2005;%20;280:19472-9.

(20) Regan J, Capolino A, Cirillo PF, Gilmore T, Graham AG, Hickey E, et al. Structure-activity relationships of the p38alpha MAP kinase inhibitor 1-(5-tert-butyl-2-p-tolyl-2H-pyrazol-3-yl)-3-[4-(2-morpholin-4-yl-ethoxy)naph- thalen-1-yl]urea (BIRB 796). J Med Chem 2003;46:4676-86.

(21) Zhang T, Inesta-Vaquera F, Niepel M, Zhang J, Ficarro SB, Machleidt T, et al. Discovery of potent and selective covalent inhibitors of JNK. Chem Biol 2012;19:140-54.

(22) Batey MA, Zhao Y, Kyle S, Richardson C, Slade A, Martin NM, et al. Preclinical evaluation of a novel ATM inhibitor, KU59403, in vitro and in vivo in p53 functional and dysfunctional models of human cancer. Mol Cancer Ther 2013;12:959-67.

(23) Rushworth SA, Bowles KM, Raninga P, MacEwan DJ. NF-kappaB-inhibited acute myeloid leukemia cells are rescued from apoptosis by heme oxygenase-1 induction. Cancer Res 2010;70:2973-83.

(24) Xu F, Wang F, Yang T, Sheng Y, Zhong T, Chen Y. Differential drug resistance acquisition to doxorubicin and paclitaxel in breast cancer cells. Cancer Cell International 2014;14:538.

(25) Bailey TL, Elkan C. Fitting a mixture model by expectation maximization to discover motifs in biopolymers. Proc Int Conf Intell Syst Mol Biol 1994;2:28-36.:28-36.

(26) Karolchik D, Hinrichs AS, Furey TS, Roskin KM, Sugnet CW, Haussler D, et al. The UCSC Table Browser data retrieval tool. Nucleic Acids Res 2004;32:D493-D496.

(27) Arava Y, Wang Y, Storey JD, Liu CL, Brown PO, Herschlag D. Genome-wide analysis of mRNA translation profiles in Saccharomyces cerevisiae. PNAS 2003;100:3889-94.

(28) Piques M, Schulze WX, Höhne M, Usadel Br, Gibon Y, Rohwer J, et al. Ribosome and transcript copy numbers, polysome occupancy and enzyme dynamics in Arabidopsis. Mol Syst Biol 2009;5:314.

(29) Liu MJ, Wu SH, Chen HM, Wu SH. Widespread translational control contributes to the regulation of Arabidopsis photomorphogenesis. Mol Syst Biol 2012;8:566.

(30) Spasic M, Friedel CC, Schott J, Kreth J, Leppek K, Hofmann S, et al. Genome-wide assessment of AU-rich elements by the AREScore algorithm. PLoS Genet 2012;8:e1002433.

(31) Cook KB, Kazan H, Zuberi K, Morris Q, Hughes TR. RBPDB: a database of RNA-binding specificities. Nucleic Acids Res 2011;39:D301-D308.

(32) Lee S, Truesdell SS, Bukhari SI, Lee JH, Letonqueze O, Vasudevan S. Upregulation of eIF5B controls cell-cycle arrest and specific developmental stages. Proc Natl Acad Sci U S A 2014;111:E4315-E4322.

(33) Bukhari SI, Truesdell SS, Lee S, Kollu S, Classon A, Boukhali M, et al. A Specialized Mechanism of Translation Mediated by FXR1a-Associated MicroRNP in Cellular Quiescence. Mol Cell 2016;61:760-73.

(34) Forbes SA, Beare D, Gunasekaran P, Leung K, Bindal N, Boutselakis H, et al. COSMIC: exploring the world's knowledge of somatic mutations in human cancer. Nucleic Acids Res 2015;43:D805-D811.

(35) Saito Y, Kitamura H, Hijikata A, Tomizawa-Murasawa M, Tanaka S, Takagi S, et al. Identification of therapeutic targets for quiescent, chemotherapy-resistant human leukemia stem cells. Sci Transl Med 2010;2:17ra9.

Supplemental Figures (Related to main figures 1-7)

Figure S1. Related to main figure 1. A. IC50 values of standard anti-leukemic chemotherapy, AraC, in AML cell lines (34). THP1 cell line was selected for this study as it shows strong resistance to AraC. **B.** Flow cytometric profiles of S+, SS and AraCS using BrdU and PI staining. **C.** G0 arrest of serum-starved THP1 is assessed by Western analysis of p27 and Hes1 levels. **D.** Polysome profiles of S+, SS (serum starvation for 4 hours, 1 day, 2 days and 4 days) and AraCS (5 μM AraC treatment for 3 days and 9 days) THP1 cells. Heavy polysomes (≥3 ribosomes)-associated mRNAs were analyzed by microarray. 'P/M' indicates polysome to monosome ratios. **E.** Gene ontology analysis of differentially expressed genes at the translatome level in response to serum starvation. The statistical significance of enriched gene ontology categories is shown as a heap map. **F.** Scatter plots (i), Principal component analysis (PCA) analysis (ii) and unbiased hierarchical clustering (iii) of the translatomes of cells that were serum-starved for indicated times. **G.** Heatmap and boxplot of the expression of LSC gene signature (35) in AraCS and SS cells. See also main Figure 1.

Figure S2. Related to main figure 2. A. Western analysis of p27KIP1 (p27) in S+ and SS cells as a marker for G0/G1 arrest, shows that G0 cells are induced by serum-starvation in a number of cancer cell lines. **B.** G0 arrest of serum-starved MCF7 is assessed by Western analysis of p27 and Hes1 levels. **C**. Flow cytometric analysis of S+ and SS cells from MCF7 using BrdU and PI staining. **D.** Polysome profiles of S+ and SS cells from MCF7, U2OS, HepG2 and non-cancerous HFF fibroblasts cell lines. Heavy polysomes (≥ 3 ribosomes) were analyzed by microarray. **E.** GSEA shows gene categories regulated commonly in the proteome or translatome of G0 cells from five different cell types. Heatmap of normalized enrichment score (NES) is shown. 'N' marks the limited resolution of the proteome in the

GSEA. **F.** PCA analysis (i) and unbiased hierarchical clustering (ii) of the translatomes of SS or AraCS cells from five different cell lines are shown. **G**. Heatmap and boxplot of the expression of SASP signature genes in SS and AraCS THP1 cells. **H**. Heatmap showing the expression of ER-stress related genes in SS and AraCS cells. **I**. Bar graphs showing the expression of CD47 and HLA-G in S+, SS and AraCS cells. *$P \leq 0.05$ Data are represented as average ± SEM. See also main Figure 2.

Figure S3. Related to main Figure 3. A. Distinct motifs enriched in 5' UTRs of genes where ribosome occupancy is significantly increased (ΔRO↑, top panel) or decreased (ΔRO↓, bottom panel) in G0 chemoresistant cells. **B**. Minimum free energy of RNA secondary structure and length of 5'UTRs of genes. **C**. GSEA showing the expression of genes involved in the decay of ARE mRNAs in SS THP1 (top) or SS MCF7 (bottom) compared to S+ cells. **D.** Heatmap of the expression of exosome complex genes (3'-5' exonuclease RNA decay and processing complex) in G0 cancer cells. **E.** Boxplot showing reduced expression of proteasome complex genes in G0 leukemic cells. **F.** Expression of known ARE-binding proteins in G0 leukemic cells are shown as a heatmap. These proteins are known to cause ARE mRNA decay or translation repression. Data are represented as average ± SEM. See also main Figure 3.

Figure S4. Related to main Figure 4. A. Flow cytometric profiles of MV4:11 or MOLM13 cells treated with AraC or AraC plus LY2228820. Percentages of BrdU-positive cells are shown. **B**. Effect of p38 MAPK inhibition on survival of AraC-resistant cells. MOLM13 leukemic cells were pre-treated with various concentrations of BIRB796 (BB), followed by AraC or vehicle treatment. Cell viability and death were assessed by cell counting, MTS and caspase 3/7 assays. *$P \leq 0.05$ Data are represented as average ± SEM. See also main Figure 4.

Figure S5. Related to main Figures 5 and 6. A. TNF-R1 and TNF-R2 expression at the translatome level. **B**. Translatome expression of BCL2A1, BCL3 and BCL6 at indicated time points after serum starvation. **C**. Flow cytometric profiles of THP1 cells treated with vehicle or recombinant TNFα. **D**. Cell viability and death of THP1 cells pre-treated with 300 μg/ml PFD for indicated time followed by 5 μM AraC. **E**. Combined effect of PFD and TNFα shRNA on chemotherapy survival. Cell viability and cell death assay were performed with THP1 cells in which the shRNA against TNFα or control shRNA was induced 3 days before AraC treatment, with or without 300 μg/ml of PFD added 1 day before AraC treatment. **F.** MOLM13-GFP-luciferase cells were cultured with or without HS-27 cells and treated with PLA therapy or AraC. Representative microscopic images (top panel) and quantification of luciferase activity (bottom panel) are shown. **G**. TNFα expression at the translatome (top) and RNA levels (bottom) in SS cells treated with vehicle or PFD. **H**. MCF7 cells were pre-treated with 300 μg/ml PFD or vehicle 1 day before treatment with serum starvation or 150 nM doxorubicin. Cell viability of PFD-treated compared to vehicle-treated cells is shown. $*P \leq 0.05$ Data are represented as average ± SEM. See also main Figures 5-6.

Figure S6. Related to main Figures 1-7. A model of chemoresistance in AML. Post-transcriptional and translational regulation of gene expression that leads to chemoresistance and G0 cell survival, is regulated by DNA damage and stress signaling—that is triggered in subpopulations of cancer by genomic instability and stress, as well as induced by chemotherapy and serum-starvation. See also main Figures 1-7.

Supplemental Table S1. Related to main Figures 1-7. Genes up-regulated at the translatome level in both AraC and SS cells.

Supplemental Table S2. Related to main Figures 1-7. Genes bearing AU-rich elements (AREs) and up-regulated at the translatome level.

Figure S1

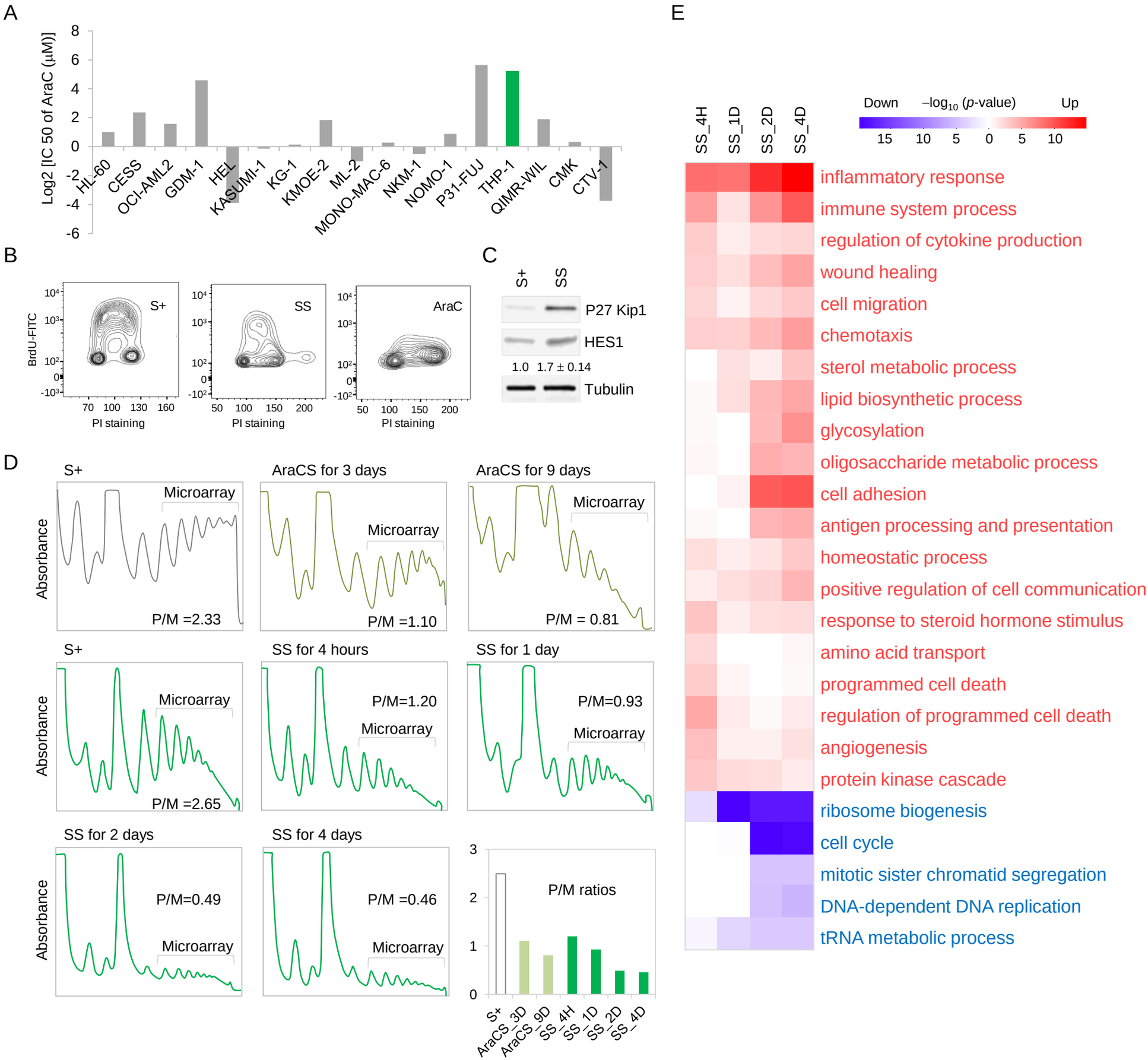
A
Log2 [IC 50 of AraC (μM)]
HL-60
CESS
OCI-AML2
GDM-1
HEL
KASUMI-1
KG-1
KMOE-2
ML-2
MONO-MAC-6
NKM-1
NOMO-1
P31-FUJ
THP-1
QIMR-WIL
CMK
CTV-1
B
S+
SS
AraC
BrdU-FITC
PI staining
C
S+
SS
P27 Kip1
HES1
1.0
1.7 ± 0.14
Tubulin
D
S+
AraCS for 3 days
AraCS for 9 days
Microarray
P/M =2.33
P/M =1.10
P/M = 0.81
SS for 4 hours
SS for 1 day
P/M=1.20
P/M=0.93
P/M =2.65
SS for 2 days
SS for 4 days
P/M=0.49
P/M =0.46
Absorbance
P/M ratios
S+
AraCS_3D
AraCS_9D
SS_4H
SS_1D
SS_2D
SS_4D
E
SS_4H
SS_1D
SS_2D
SS_4D
Down
–log10 (p-value)
Up
15
10
5
0
5
10
inflammatory response
immune system process
regulation of cytokine production
wound healing
cell migration
chemotaxis
sterol metabolic process
lipid biosynthetic process
glycosylation
oligosaccharide metabolic process
cell adhesion
antigen processing and presentation
homeostatic process
positive regulation of cell communication
response to steroid hormone stimulus
amino acid transport
programmed cell death
regulation of programmed cell death
angiogenesis
protein kinase cascade
ribosome biogenesis
cell cycle
mitotic sister chromatid segregation
DNA-dependent DNA replication
tRNA metabolic process

F

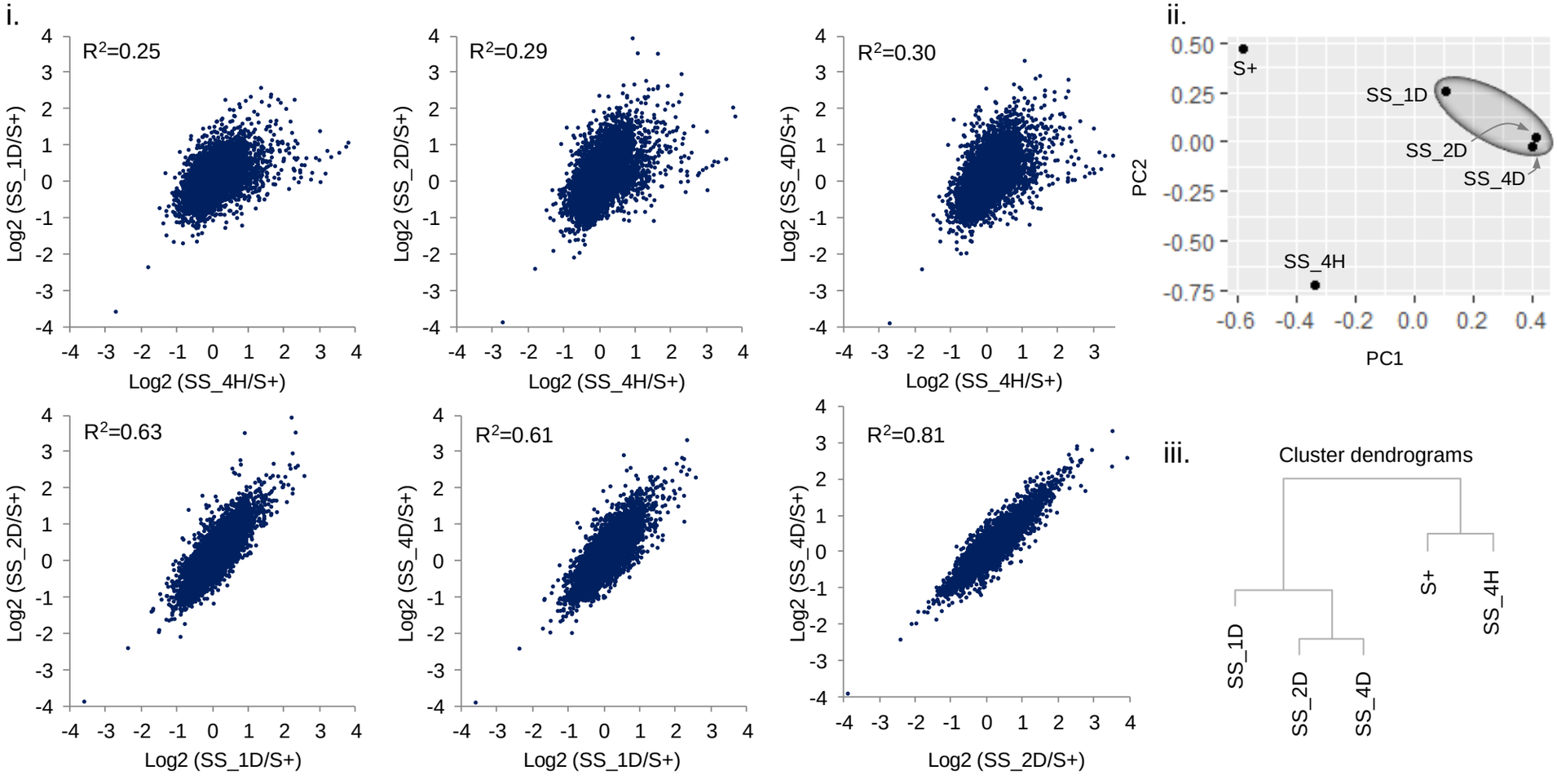
i.
R²=0.25
R²=0.29
R²=0.30
R²=0.63
R²=0.61
R²=0.81
Log2 (SS_1D/S+)
Log2 (SS_2D/S+)
Log2 (SS_4D/S+)
Log2 (SS_4H/S+)
Log2 (SS_1D/S+)
Log2 (SS_1D/S+)
Log2 (SS_2D/S+)
ii.
S+
SS_1D
SS_2D
SS_4D
SS_4H
PC1
PC2
iii.
Cluster dendrograms
S+
SS_4H
SS_1D
SS_2D
SS_4D

G

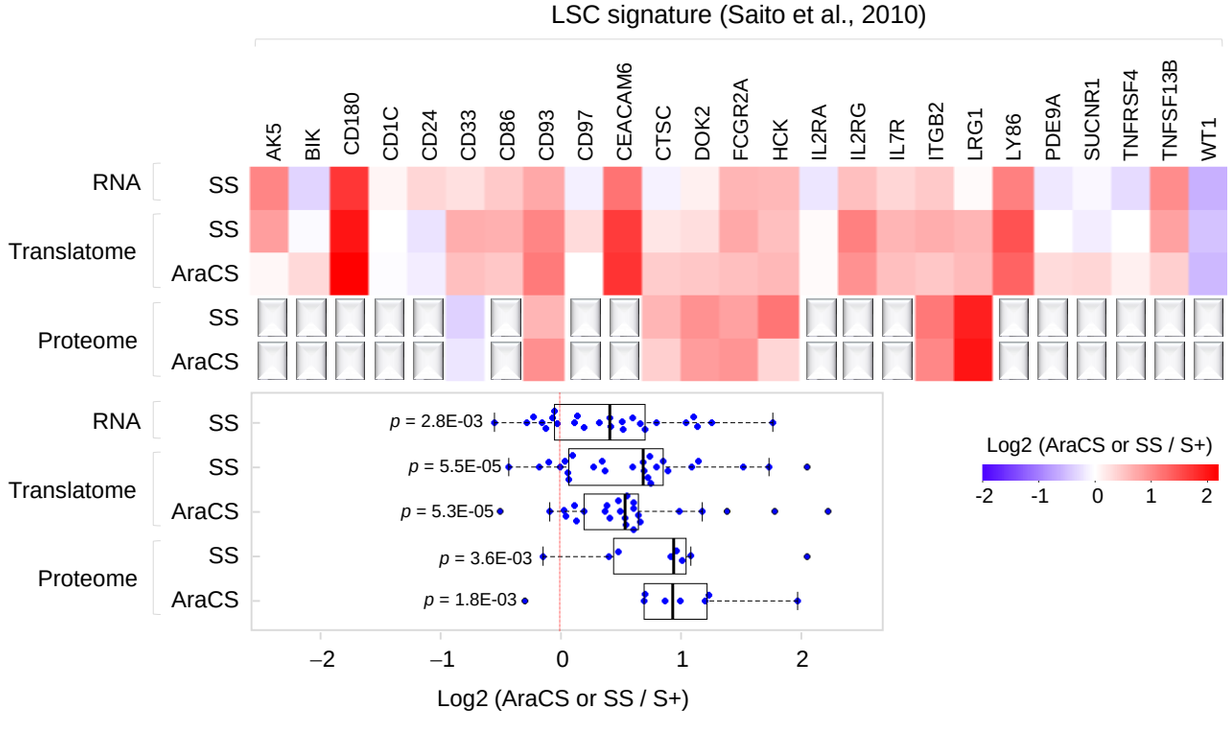
LSC signature (Saito et al., 2010)
AK5
BIK
CD180
CD1C
CD24
CD33
CD86
CD93
CD97
CEACAM6
CTSC
DOK2
FCGR2A
HCK
IL2RA
IL2RG
IL7R
ITGB2
LRG1
LY86
PDE9A
SUCNR1
TNFRSF4
TNFSF13B
WT1
RNA
Translatome
Proteome
SS
AraCS
p = 2.8E-03
p = 5.5E-05
p = 5.3E-05
p = 3.6E-03
p = 1.8E-03
Log2 (AraCS or SS / S+)
Log2 (AraCS or SS / S+)

Figure S2

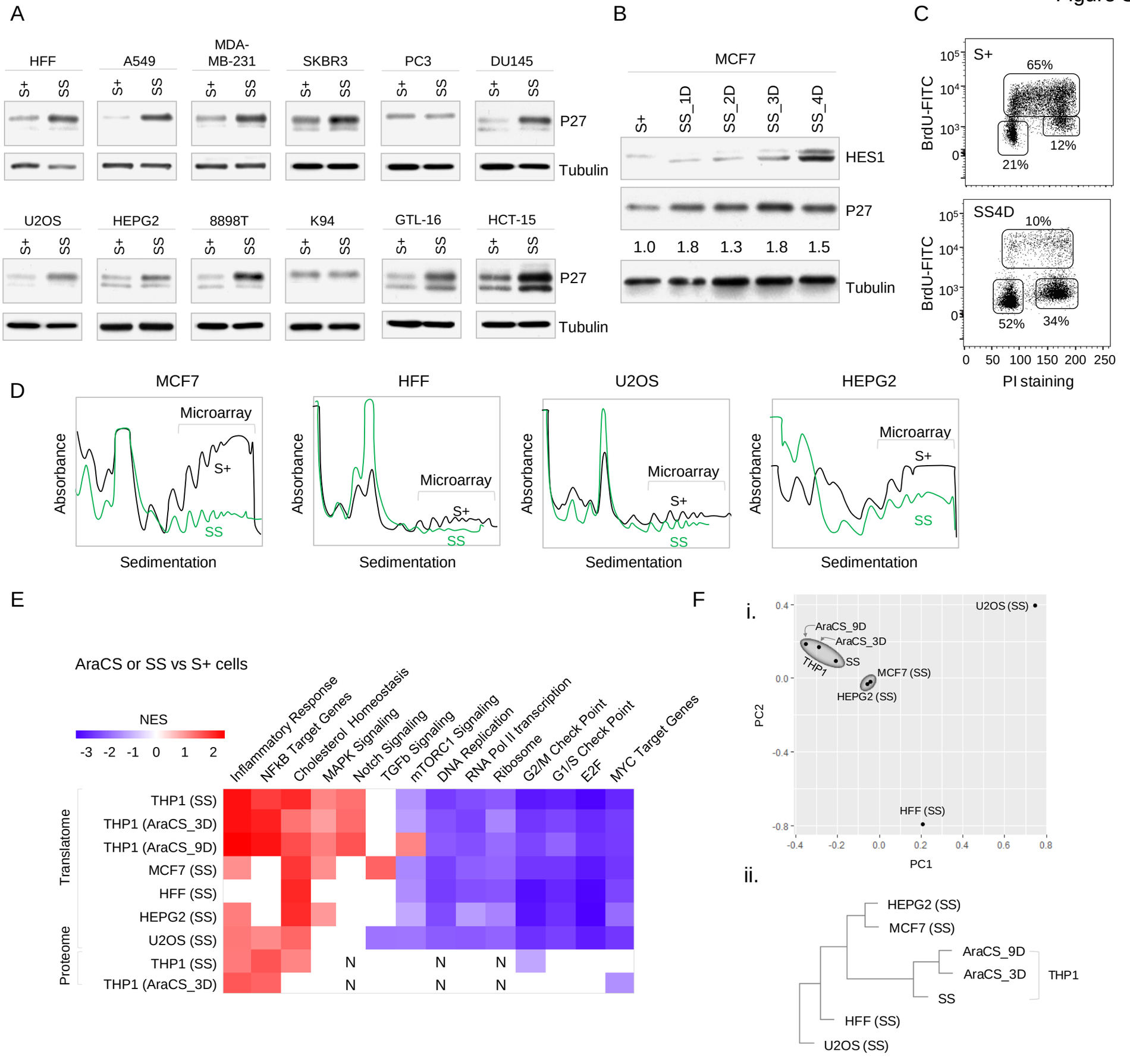
A
HFF
A549
MDA-MB-231
SKBR3
PC3
DU145
S+
SS
P27
Tubulin
U2OS
HEPG2
8898T
K94
GTL-16
HCT-15
B
MCF7
S+
SS_1D
SS_2D
SS_3D
SS_4D
HES1
P27
1.0 1.8 1.3 1.8 1.5
Tubulin
C
S+
65%
12%
21%
SS4D
10%
52%
34%
BrdU-FITC
PI staining
D
MCF7
HFF
U2OS
HEPG2
Microarray
S+
SS
Absorbance
Sedimentation
E
AraCS or SS vs S+ cells
NES
-3 -2 -1 0 1 2
Inflammatory Response
NFkB Target Genes
Cholesterol Homeostasis
MAPK Signaling
Notch Signaling
TGFb Signaling
mTORC1 Signaling
DNA Replication
RNA Pol II transcription
Ribosome
G2/M Check Point
G1/S Check Point
E2F
MYC Target Genes
Translatome
Proteome
THP1 (SS)
THP1 (AraCS_3D)
THP1 (AraCS_9D)
MCF7 (SS)
HFF (SS)
HEPG2 (SS)
U2OS (SS)
THP1 (SS)
THP1 (AraCS_3D)
N
F
i.
U2OS (SS)
AraCS_9D
AraCS_3D
SS
THP1
MCF7 (SS)
HEPG2 (SS)
HFF (SS)
PC1
PC2
ii.
HEPG2 (SS)
MCF7 (SS)
AraCS_9D
AraCS_3D
THP1
SS
HFF (SS)
U2OS (SS)

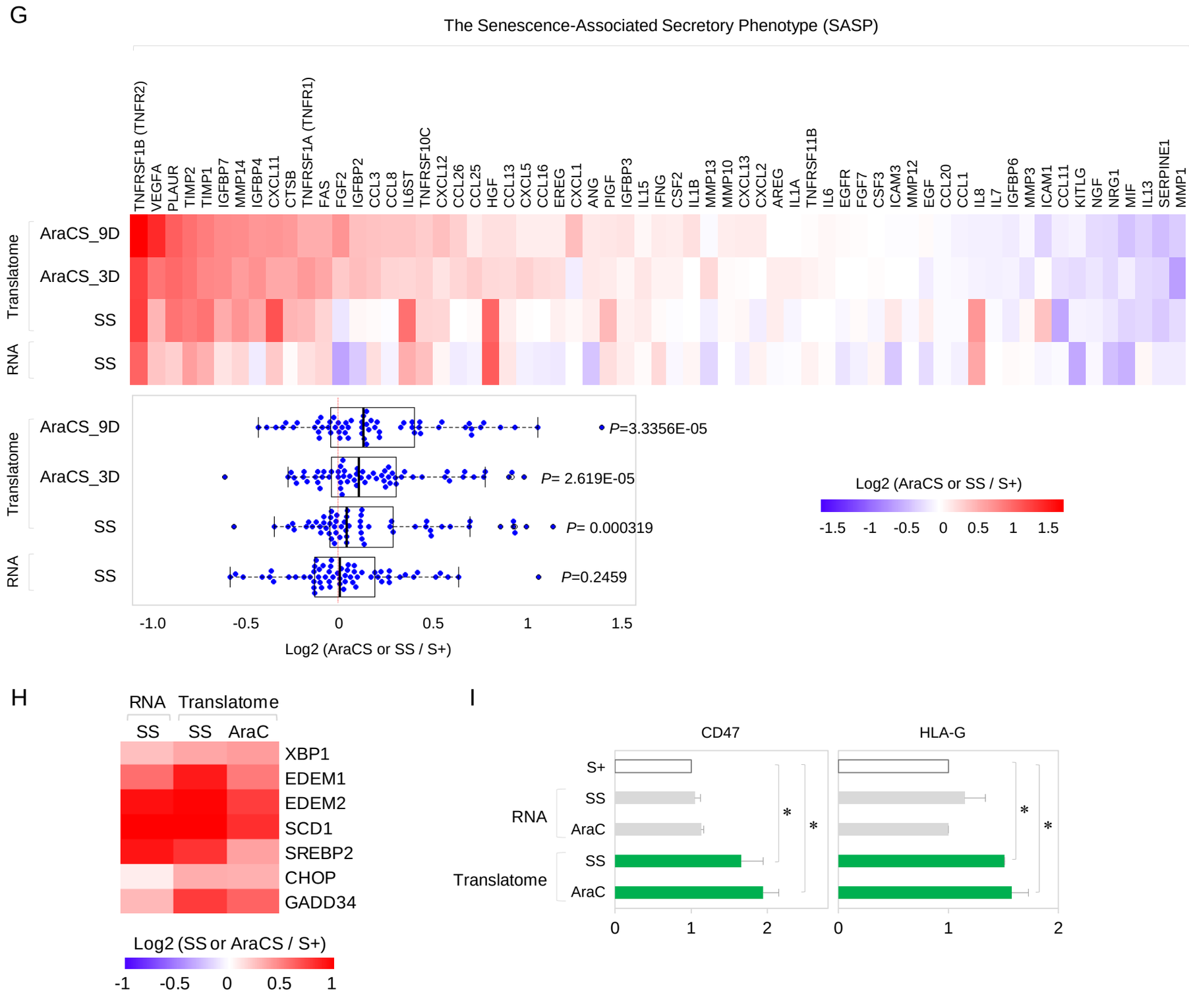
G
The Senescence-Associated Secretory Phenotype (SASP)
TNFRSF1B (TNFR2)
VEGFA
PLAUR
TIMP2
TIMP1
IGFBP7
MMP14
IGFBP4
CXCL11
CTSB
TNFRSF1A (TNFR1)
FAS
FGF2
IGFBP2
CCL3
CCL8
IL6ST
TNFRSF10C
CXCL12
CCL26
CCL25
HGF
CCL13
CXCL5
CCL16
EREG
CXCL1
ANG
PIGF
IGFBP3
IL15
IFNG
CSF2
IL1B
MMP13
MMP10
CXCL13
CXCL2
AREG
IL1A
TNFRSF11B
IL6
EGFR
FGF7
CSF3
ICAM3
MMP12
EGF
CCL20
CCL1
IL8
IL7
IGFBP6
MMP3
ICAM1
CCL11
KITLG
NGF
NRG1
MIF
IL13
SERPINE1
MMP1
Translatome
RNA
AraCS_9D
AraCS_3D
SS
SS
P=3.3356E-05
P= 2.619E-05
P= 0.000319
P=0.2459
-1.0
-0.5
0
0.5
1
1.5
Log2 (AraCS or SS / S+)
Log2 (AraCS or SS / S+)
-1.5
-1
-0.5
0
0.5
1
1.5
H
RNA
Translatome
SS
SS
AraC
XBP1
EDEM1
EDEM2
SCD1
SREBP2
CHOP
GADD34
Log2 (SS or AraCS / S+)
-1
-0.5
0
0.5
1
I
CD47
HLA-G
S+
SS
AraC
SS
AraC
RNA
Translatome
*
*
*
*
0
1
2
0
1
2

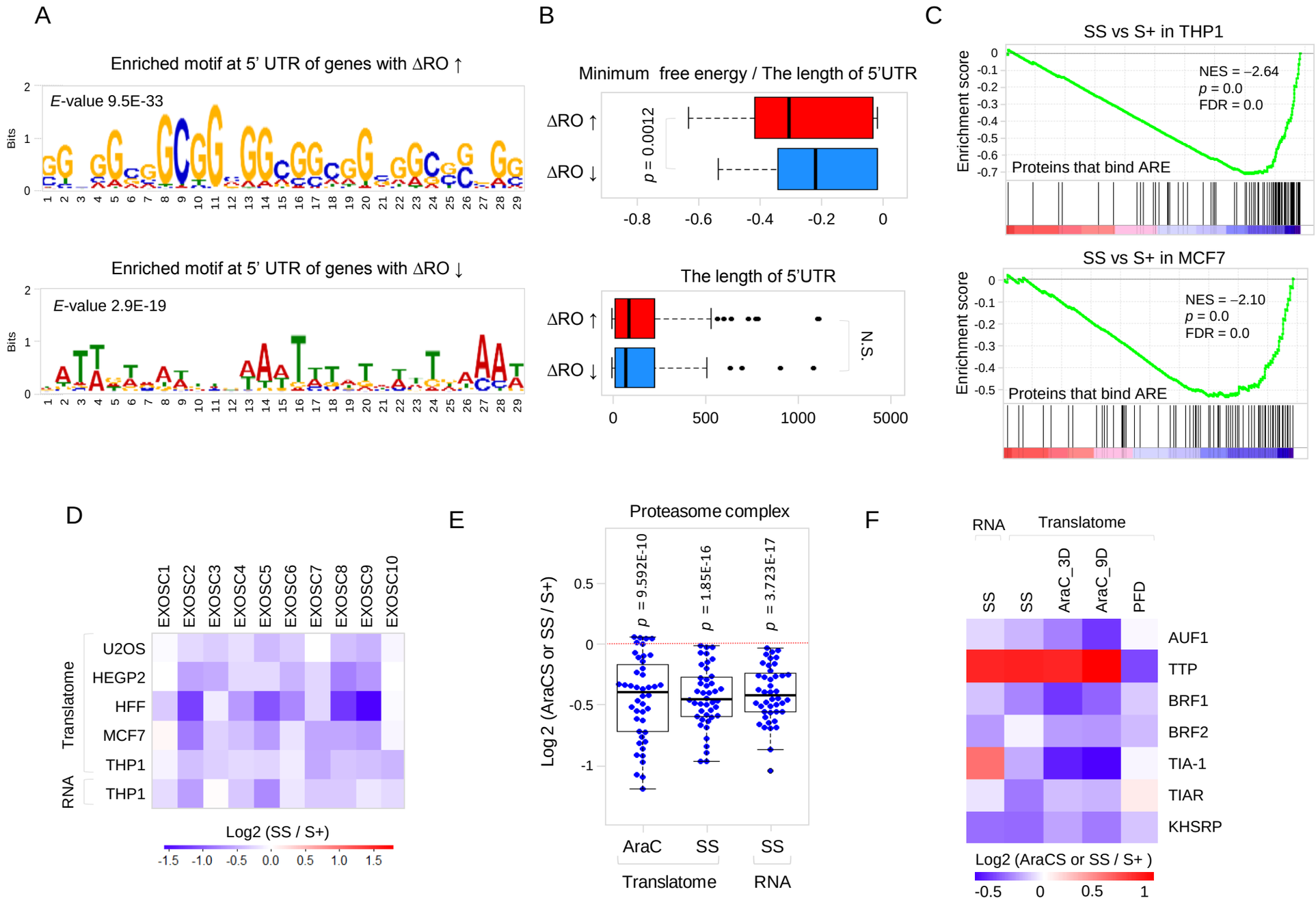
A
Enriched motif at 5' UTR of genes with ΔRO ↑
E-value 9.5E-33
Bits
Enriched motif at 5' UTR of genes with ΔRO ↓
E-value 2.9E-19
B
Minimum free energy / The length of 5'UTR
ΔRO ↑
ΔRO ↓
p = 0.0012
The length of 5'UTR
N.S.
C
SS vs S+ in THP1
Enrichment score
NES = –2.64
p = 0.0
FDR = 0.0
Proteins that bind ARE
SS vs S+ in MCF7
NES = –2.10
p = 0.0
FDR = 0.0
D
EXOSC1
EXOSC2
EXOSC3
EXOSC4
EXOSC5
EXOSC6
EXOSC7
EXOSC8
EXOSC9
EXOSC10
Translatome
U2OS
HEGP2
HFF
MCF7
THP1
RNA
THP1
Log2 (SS / S+)
E
Proteasome complex
Log 2 (AraCS or SS / S+)
p = 9.592E-10
p = 1.85E-16
p = 3.723E-17
AraC
SS
SS
Translatome
RNA
F
RNA
Translatome
SS
SS
AraC_3D
AraC_9D
PFD
AUF1
TTP
BRF1
BRF2
TIA-1
TIAR
KHSRP
Log2 (AraCS or SS / S+)

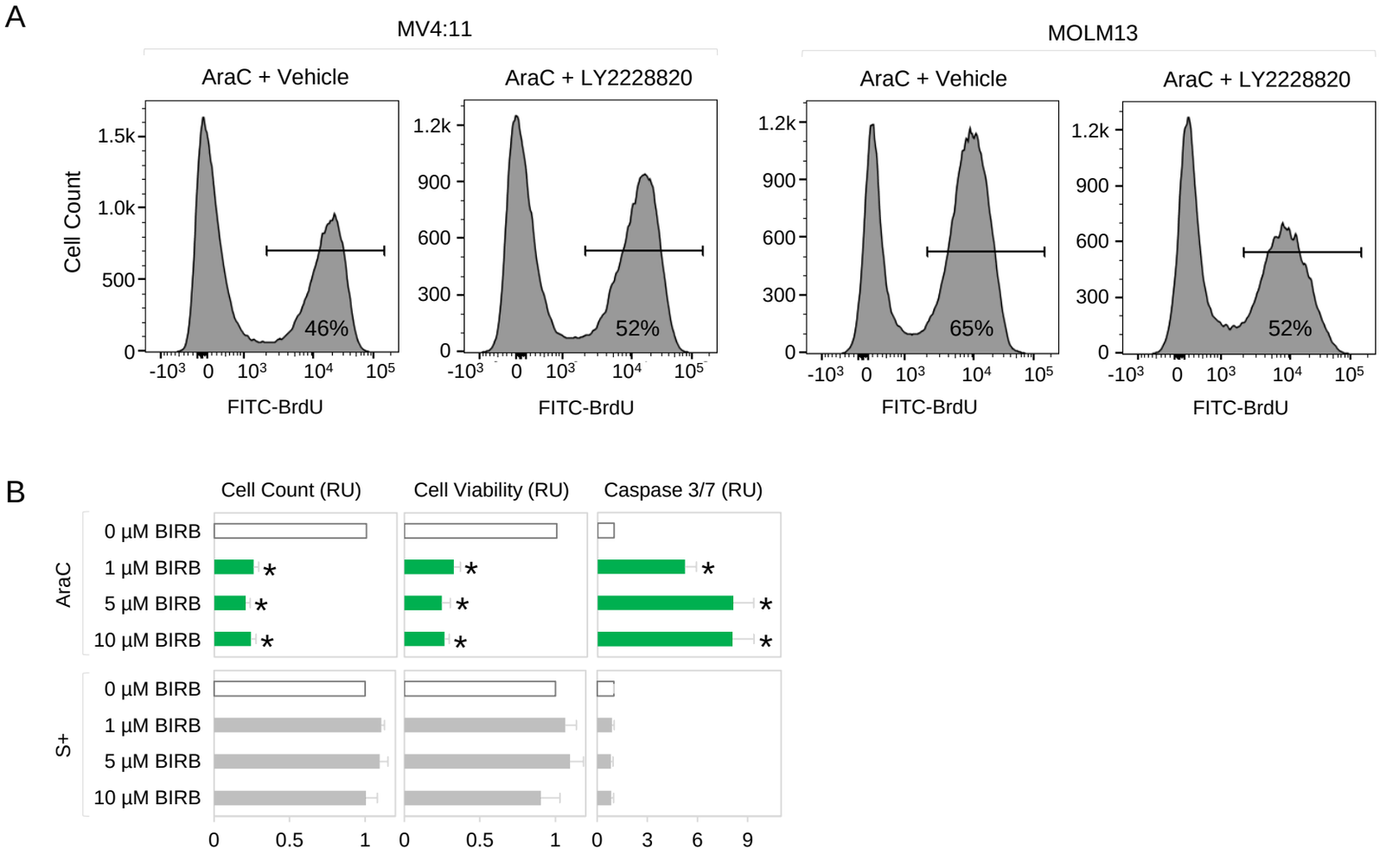
A
MV4:11
MOLM13
AraC + Vehicle
AraC + LY2228820
AraC + Vehicle
AraC + LY2228820
Cell Count
1.5k
1.0k
500
0
1.2k
900
600
300
0
46%
52%
65%
52%
-10³ 0 10³ 10⁴ 10⁵
FITC-BrdU
B
Cell Count (RU)
Cell Viability (RU)
Caspase 3/7 (RU)
AraC
S+
0 µM BIRB
1 µM BIRB
5 µM BIRB
10 µM BIRB
*
0 0.5 1
0 3 6 9

Figure S5

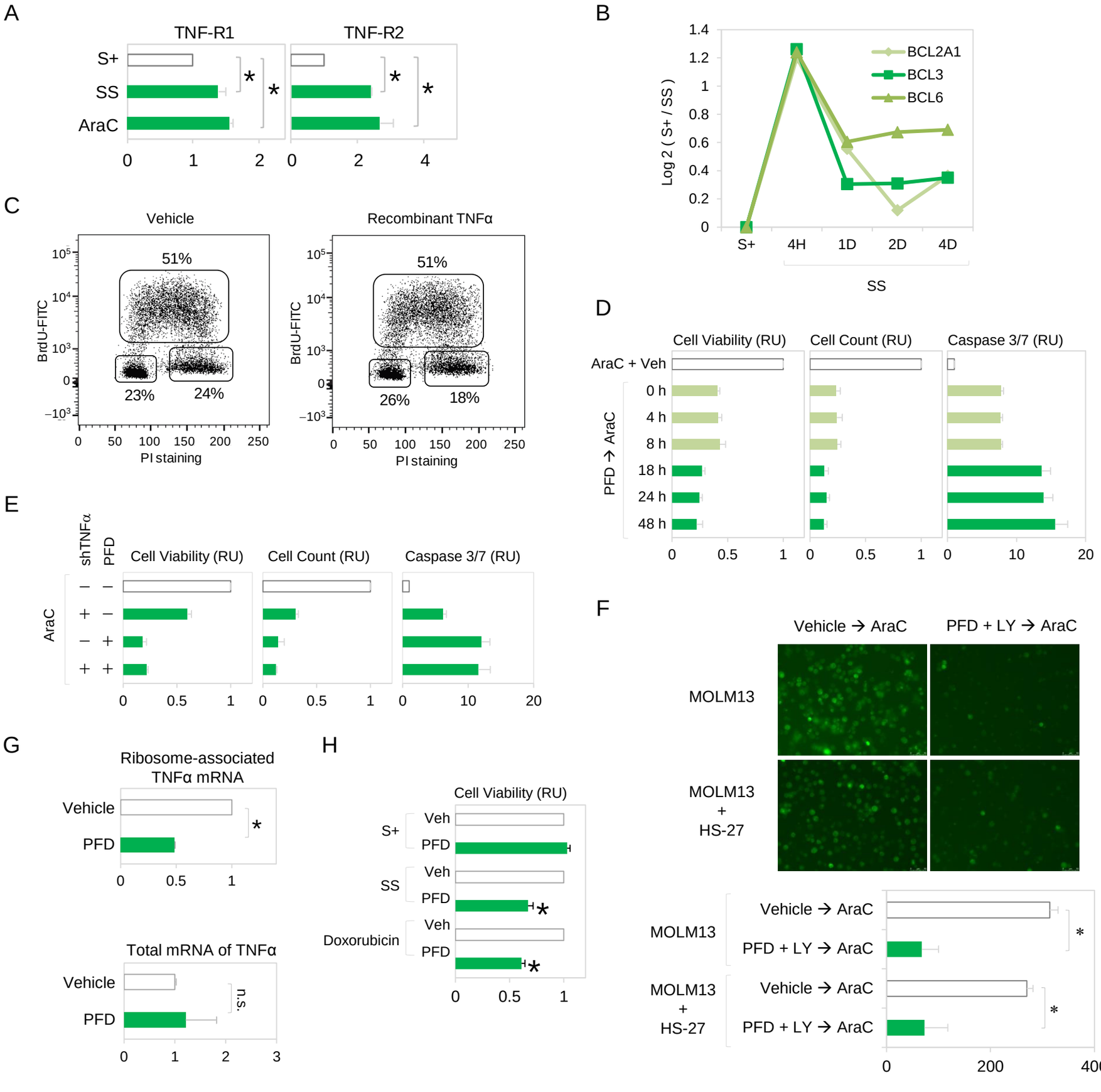
A
TNF-R1
TNF-R2
S+
SS
AraC
B
Log 2 (S+ / SS)
BCL2A1
BCL3
BCL6
S+
4H
1D
2D
4D
SS
C
Vehicle
Recombinant TNFα
BrdU-FITC
PI staining
51%
23%
24%
26%
18%
D
Cell Viability (RU)
Cell Count (RU)
Caspase 3/7 (RU)
AraC + Veh
PFD → AraC
0 h
4 h
8 h
18 h
24 h
48 h
E
shTNFα
PFD
AraC
F
Vehicle → AraC
PFD + LY → AraC
MOLM13
MOLM13 + HS-27
G
Ribosome-associated TNFα mRNA
Total mRNA of TNFα
Vehicle
PFD
n.s.
H
Cell Viability (RU)
S+
SS
Doxorubicin
Veh
PFD

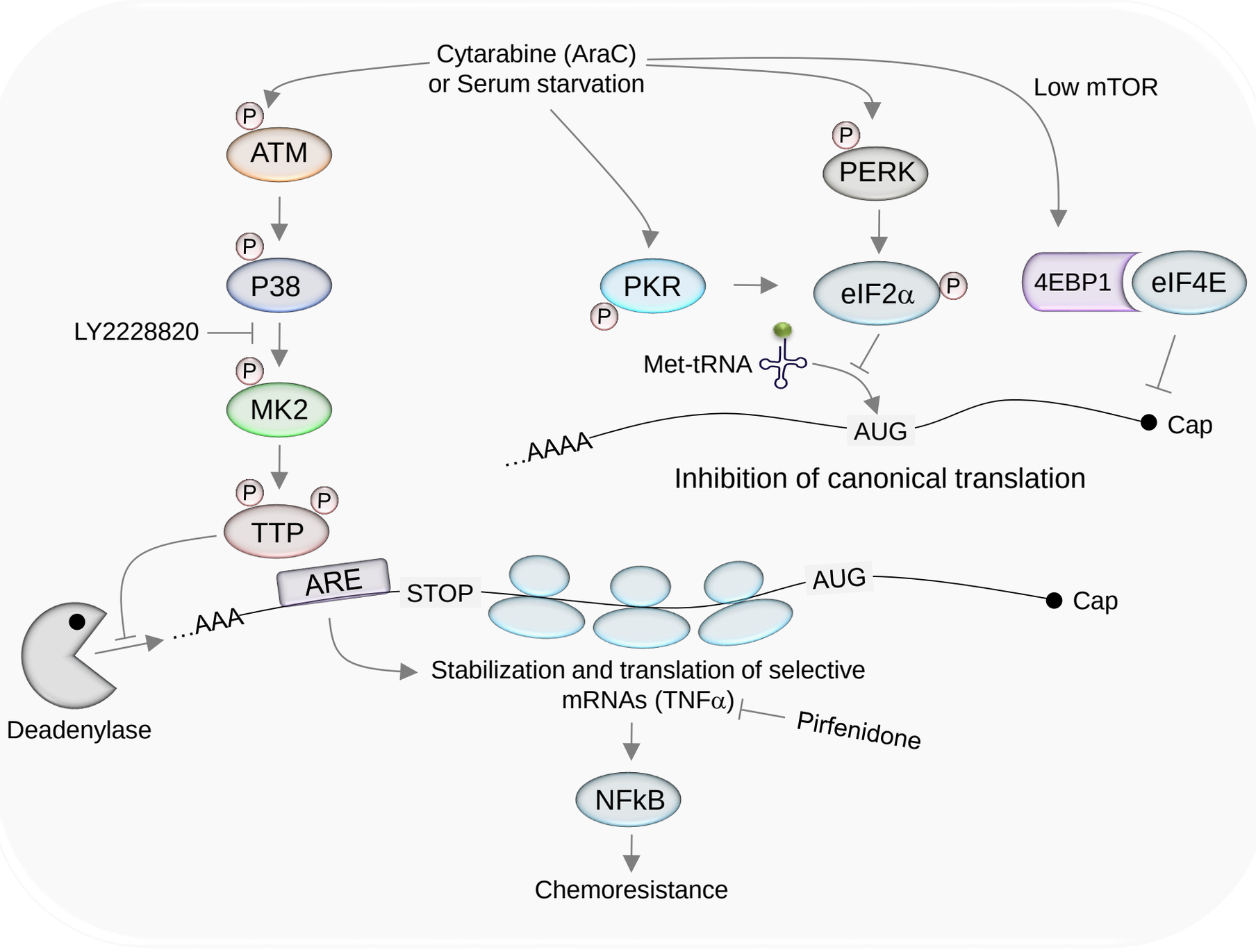
Cytarabine (AraC)
or Serum starvation
Low mTOR
P
ATM
P
P38
LY2228820
P
MK2
P
P
TTP
P
PERK
PKR
P
eIF2α
P
4EBP1
eIF4E
Met-tRNA
AUG
Cap
…AAAA
Inhibition of canonical translation
ARE
STOP
AUG
Cap
…AAA
Deadenylase
Stabilization and translation of selective
mRNAs (TNFα)
Pirfenidone
NFkB
Chemoresistance